Energy 247 (2022) 123322

Contents lists available at ScienceDirect

Energy

journal homepage: www.elsevier.com/locate/energy

Wave excitation force forecasting using neural networks

Kumars Mahmoodi, PhD [a, *], Erivelton Nepomuceno [a], Abolhassan Razminia [b]

[a] Centre for Ocean Energy Research, Department of Electronic Engineering, Maynooth University, Ireland
[b] Department of Electrical Engineering, Faculty of Intelligent Systems Engineering and Data Science, Persian Gulf University, Bushehr, Iran

ARTICLE INFO

Article history:
Received 28 March 2021
Received in revised form
16 December 2021
Accepted 26 January 2022
Available online 28 January 2022

Keywords:
Wave energy conversion
Wave excitation force
Nonlinear autoregressive
Group method of data handling
Long short-term memory

ABSTRACT

Many wave energy conversion applications require future knowledge or forecasting of the wave excitation force values. Most wave energy converter (WEC) control strategies need to forecast the time-series excitation force for wave energy harvesting maximization. The main aim of this study is to forecast the wave excitation force experiences by a two-body heaving point absorber WEC (as a case study) using three forecasting neural network methods. The wave excitation force is calculated based on the hydrodynamic characteristics of the considered device in the frequency and time-domain simulations. The nonlinear autoregressive neural (NAR) network, group method of data handling (GMDH) network, and Long Short-Term Memory (LSTM) network are fitted to the wave elevation time-series data to forecast the future values of the excitation force. The performance of the examined methods is evaluated for various irregular incident waves that are created using different wave spectrums. Moreover, sensitivity analyses to sampling period and algorithms input parameters are performed to investigate the accuracy and generalizability of the discussed methods at different conditions. Each data set is divided into training and test sets. The results show that the performance of all discussed methods is satisfactory in training data sets and short-term ahead forecasting, but the NAR network method provides a relatively better agreement with test target data compared to other methods.

1. Introduction

The excitation force produces by the integral of the water pressure over the wetted surface of the WEC bodies [1]. Thus, it is possible to control the WEC motions by controlling the wave excitation force using tuning the wetted surface of the bodies to improve the amount of power absorbed by the system. In most control methods, the highest power production obtains when the velocity phase of the WEC motion appropriately matches the wave excitation force phase [2,3]. Therefore, the accurate estimation of the wave excitation force is necessary for most power maximization control strategies and wave energy conversion applications to address the WECs economic problems. Moreover, there is no need to use additional expensive hardware to increase the output power of the device.

Some control methods require some knowledge of the incident wave elevation and wave excitation force values to determine what control actions will maximize the output power. Especially in optimal control problems, a short time forecasting of the wave elevation or wave excitation force is essential to this controller method [4], since the control problem is dependent on a reference strategy which determined from wave excitation force values [5]. As another example, the reactive control strategies require transferring some force into the WEC bodies to keep the velocity and the excitation force in phase [1]. This force can be determined based on the future values of the wave excitation force. In the resistive control strategies, the power take-off (PTO) damping coefficient and as a result, the PTO force can be estimated based on the incident wave elevation or wave excitation force for each sea state. Phase and amplitude control strategies control the device velocity in phase with the wave excitation force, and the amplitude is also regulated based on the wave elevation [6]. According to the stated cases, future knowledge of the excitation force value may be required for various control schemes because most of the control reactions are regulated according to its characteristics. While excitation force estimation is comfortable for regular waves, it is

* Corresponding author.
E-mail addresses: kumars.mahmoodi@mu.ie (K. Mahmoodi), erivelton.nepomuceno@mu.ie (E. Nepomuceno), razminia@pgu.ac.ir (A. Razminia).

https://doi.org/10.1016/j.energy.2022.123322
0360-5442/

more complicated for real irregular sea states. Therefore, the WEC controller design is a challenging problem in practical usages and relies on the accuracy of excitation force estimation and forecasting.

Some attempts are made to predict and forecast the wave elevation or wave excitation force by various methods. Ref. [7] presented an approach for the short-term wave forecasting for real-time control of WECs using different methods including cyclical mode, sinusoidal extrapolation with the extended Kalman filter, autoregressive, and neural networks. A study of the prediction requirements in real-time control of WECs presented in Ref. [8]. In this research, the predictability of the excitation force was determined using stochastic autoregressive models. Ref. [9] presented a comparison of the available excitation force estimators for WEC devices found in the literature. Eleven estimation strategies were compared based on the required input data, achieved accuracy, computational delay, and estimation time. Ref. [10] applied a recursive least squares filter to predict the wave excitation force future values of a generic heaving WEC based on the measured water surface elevation data collected from the Oregon Coast.

A methodology suggested in Ref. [11] to construct an excitation force estimator using a Kalman filter and a forecaster using an autoregressive model for a heaving buoy WEC. Ref. [12] forecasted the wave excitation force based on its past estimated values using two different autoregressive models for one body and arrays of wave energy devices. Ref. [13] developed two forecasting algorithms, the approximate Prony method based on ESPRIT and SVM regression, for wave elevations and wave excitation forces to apply feed-forward controllers on offshore floating wind turbines. A wave excitation force prediction methodology for a sliding crank PTO was presented in Ref. [14] based on autoregressive filters. A deterministic wave excitation force estimator was proposed based on the fast unknown input estimation concept in Ref. [15]. A new strategy with combining the observer-based unknown input estimator (OBUIE) and Gaussian Process (GP) model was adopted in Ref. [16] to wave excitation force estimation and forecasting for WEC power conversion maximization. First, the OBUIE was used to estimate the wave excitation force, then the GP model was applied to forecast the wave excitation force.

According to our best knowledge of the literature, classical statistical techniques are used to the wave excitation force forecasting that are not accurate enough and are not useful in practice due to the very high nonlinear nature of the waves. The lack of a comprehensive study to investigate different machine learning approaches to forecast the wave excitation force is visible. Applying more advanced new solutions, especially machine learning methods, can be very useful and promise new horizons in this area. Therefore, this study aims to develop a future excitation force forecasting strategy based on machine learning methods with the potential for WEC power maximization control applications. To this accomplishment, NAR, GMDH, and LSTM networks are used to forecast the future wave excitation force values based on the past wave elevation data. The final goal of this research is to suggest the best methods for forecasting the future values of the wave excitation force acting on the wetted surface of the WEC bodies.

The following sections are organized as follows. The details of the proposed methodology, considered WEC, a brief introduction to the hydrodynamic modeling, machine learning forecasting methods, performance evaluation criteria and data sets are presented in Section 2. In Section 3, the performance of different considered machine learning methods in forecasting the wave elevation and wave excitation force on the train and test data sets is computed and compared. Finally, in Section 4, the main conclusions of this study and the future outlooks are drawn.

2. Data and methodology

2.1. Proposed methodology

Block diagram of the proposed methodology for forecasting the wave excitation force using considered machine learning approaches is presented in Fig. 1. Based on this figure, at the first step, a model of a generic two-body heaving point absorber WEC is simulated as a case study in both frequency and time domains. The linear potential flow theory is used to consider hydrodynamic forces generated by the instantaneous water surface elevation and geometry of the bodies. Water surface elevation records are created using known wave spectrums. While a point absorber WEC is used to test the performance of the forecasting models, the proposed methodology is general and can be applied to any WEC design. After modeling the considered WEC, the time-domain excitation force will be estimated based on the time-series wave elevation data and hydrodynamic coefficients obtained numerically using frequency-domain boundary element method analysis. The wave elevation and wave excitation time-series forecasted by machine learning methods are compared to the real values calculated from the hydrodynamic WEC modeling. Then, the accuracy of the forecasting methods is compared to each other based on the well-known performance statistical criteria. Finally, more accurate forecasting methods are determined based on the comparison results.

The proposed methodology presented in this research is not dependent on a specific sea state and is not needed to cover all possible sea states in order to make an acceptable model. As a case study, several desired waves are generated using different available wave spectra, and the performance of machine learning methods in estimating the future values of the wave height and excitation force is measured. Therefore, it is needed to create some different time series of wave elevation records to compare the performance of the studied forecasting methods at a variety of wave conditions.

2.2. Model introduction

2.2. 1. Considered WEC

Although the proposed methodology used in this paper is generic and can be developed for different types of the WECs, a two-body heaving point absorber is considered as an example of the WEC to performance evaluation of the discussed machine learning forecasting methods. The considered device is the Reference Model 3 (RM3) [17,18] developed by the National Renewable Energy and Sandia National Laboratories. The devise schematic and its dimensions are illustrated in Fig. 2. The device is axisymmetric and consists of a floating and a reaction spar/plate bodies. The bodies only move in the heave (vertical) direction, and the output power is generated by the relative motion between the floating and the spar. More details about the considered WEC can be found in Ref. [19].

2.2. 2. Hydrodynamics of the WEC

In general, the time-domain dynamic model of the WEC device is described as follows [19,20]:

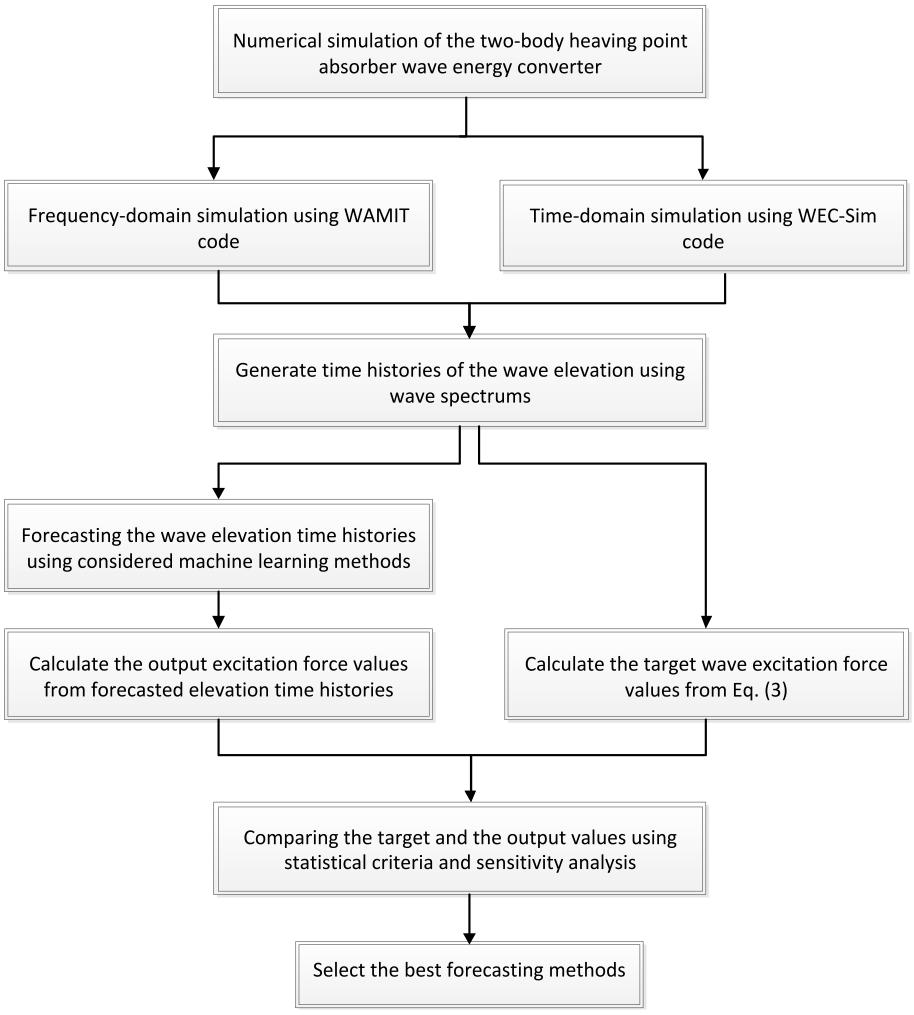

Fig. 1. Block diagram of the proposed methodology for forecasting the wave excitation force.

$$M\ddot{z}(t) = F_{hs}(t) + F_{ext}(t) + F_{rad}(t) + F_{vis}(t) + F_{pto}(t) + F_{moor}(t) \tag{1}$$

where M and t are the mass matrix and time, respectively. z, $\dot{z}$ and $\ddot{z}$ are the displacement, velocity and acceleration vector of the device, respectively. F_{hs}, F_{ext}, F_{rad}, F_{vis}, F_{pto} and F_{moor} are hydrostatic restoring force, wave excitation force, radiation force, viscous force, PTO force, and mooring force, respectively. Here, the viscous, PTO (the control input applied through the PTO device) and mooring forces are neglected for simplicity because the main purpose of this study is to provide an efficient strategy for forecasting the wave excitation force, which does not directly depend on these forces. These forces can be easily added to Eq. (1), without affecting the overall accuracy of the considered forecasting algorithms.

The hydrostatic force represented as:

$$F_{hs}(t) = -k_{hs}z(t) \tag{2}$$

where $k_{hs} = \rho g s$ is the hydrostatic coefficient, ρ and g are the water density and gravity acceleration constant, respectively; s is the body cross-sectional area of the submerged volume.

The wave excitation force can be calculated using the convolution of the wave elevation $\eta(t)$ and the non-causal excitation impulse response function (IRF), $K_{ext}(t)$, as follows:

$$F_{ext}(t) = \int_{-\infty}^{\infty} K_{ext}(t-\tau)\eta(\tau)d\tau \tag{3}$$

where

$$K_{ext}(t) = \frac{1}{2\pi}\int_{-\infty}^{\infty} X(\omega,\beta)e^{i\omega t}d\omega \tag{4}$$

where ω, β and X are the monochromatic wave frequency, wave direction and excitation force magnitude, respectively.

In this study, Eq. (3) is used to compute the target values of the excitation force for comparing the performance of the studied forecasting algorithms. This equation is a widely used formula that is applied to estimate the excitation force of the various WEC devices, which is dependent on the wave elevation. The excitation force values are essential for some of the power maximization control strategies. It should be noted that Eq. (3) may not be directly

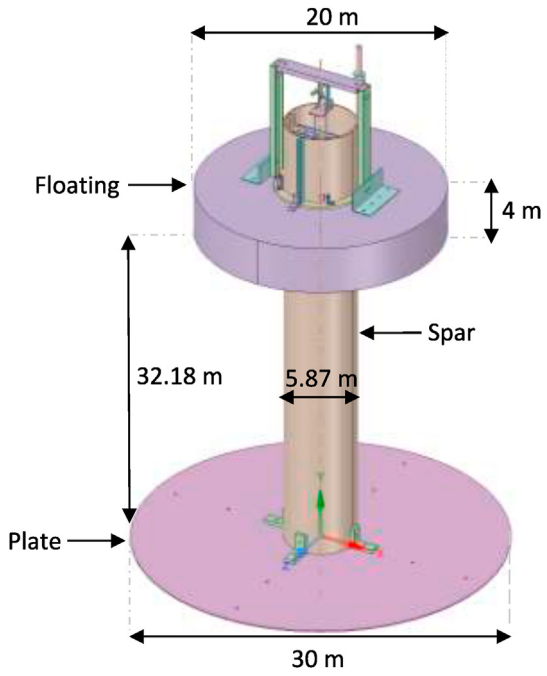

Fig. 2. Schematic diagram of the considered two-body heaving point absorber WEC and its dimensions.

used for real-time WEC control strategies, since the wave elevation should be specified at future time steps to determine what control actions will maximize the power output. Hence, the main motivation of this research is to calculate the future values of the excitation force to generating an accurate reference signal for WEC control applications.

The radiation force is the force acting on the WEC device due to the radiated waves, which can be estimated according to the following equation:

$$F_{rad}(t) = -A_{\infty}\ddot{z} - \int_0^t K_{rad}(t-\tau)\dot{z}(\tau)d\tau \tag{5}$$

where A_{∞} is the added mass matrix at the infinite frequency and K_{rad} is the radiation IRF.

2.3. Time-series forecasting methods

In this subsection, fundamental concepts and formulations of the considered forecasting approaches are reviewed.

2.3. 1. Nonlinear autoregressive neural network

Recurrent neural networks are one of the well-known machine learning methods to model nonlinear dynamic systems. NAR is one of the time delays recurrent neural networks that can identify time series patterns and nonlinear features [21,22]. It is the modified version of back-propagation multi-layer perceptron neural networks [23,24]. The output of neurons in multi-layer perceptron neural networks has the following form:

$$y_j = f\left(\sum_i w_{ij}x_i + b\right) \tag{6}$$

where w_{ij} is the weights, x_i is the input, b is the neuron's bias, y shows the output and f is the activation function.

NAR, as a dynamic machine learning method, is based on the feed-back connections through the different layers of the network. It has approximately accurate results for multi-step forward forecasting. In the first step of NAR training, none of the feed-back connection is used. However, after all the initial weights of the NAR have been determined, in the next forecasting step, the NAR needs feed-back connections that give dynamics to the network's output. As stated, the NAR training method is a modified version of the back-propagation multi-layer perceptron, where, training procedure is corresponding with random weighting on the synapses. Then, the comparison between the network outputs with target (real) values modifies the network weights. Indeed, the learning method is based on minimizing the global error between the network outputs and the target values by adjusting the network weights. In the current study, Levenberg-Marquardt (LM), Bayesian regularization (BR) and Scaled conjugate gradient (SCG) algorithms are used to adjust the network weights. The number of hidden layers and neurons are the fundamental criteria to select a proper architecture for NAR architect [25,26]. Increasing the number of hidden layers and neurons will be caused to more computational cost or overfitting. In practice, NAR with one hidden layer and an adequate number of hidden neurons has an acceptable performance [27,28].

The fundamental formulation of the NAR network to forecast the output value is as follows [29]:

$$\hat{y}(t) = f(y(t-1) + y(t-2) + \ldots + y(t-d)) \tag{7}$$

where, f is representative of a nonlinear function, t is the time and $\hat{y}$ is the considered output. Future value is related to the regressed d earlier values (i.e., feed-back delay time) of the output signal. One-step forward forecasting will be done after the training phase. To perform multi-step (p-step) forward forecasting, a closed-loop network is necessary, which has the following formulation [29]:

$$\hat{y}(t+p) = f(y(t-1) + y(t-2) + \ldots + y(t-d)) \tag{8}$$

here, p is the number of the forecasted steps.

2.3. 2. Group method of data handling network

GMDH is a self-organized heuristic machine learning approach that is introduced in Ref. [30]. GMDH, as an evolutionary computational method, is based on the sort out of the complex models and assessment of models by an external criterion on a distinct segment of the data observations. This network performs a hierarchic solution, i.e., evaluate several simple models, maintain the foremost, and iteratively structural (blocks or polynomial nodes) on them to achieve a combination of functions as the model. GMDH network has a set of neurons in each layer. Connecting the various pairs of neurons in each layer generates new neurons in the subsequent layer. The main parameters of the GMDH network, such as input variable pairs, number of hidden layers, and embedded active neurons in each layer, are automatically generated by an iterative

Table 1
The details of the wave elevation record that act on the bodies of the considered WEC device (H_s: Significant wave height, T_p: Peak period, γ: peak-shape parameter of JONSWAP spectrum).

Symbol	Generation method	Duration (s)	Sampling period (s)
W_JONS_1	JONSWAP ($H_s = 2.5\ m,\ T_p = 8\ s,\ \gamma = 3.3$)	400	0.1
W_JONS_2	JONSWAP ($H_s = 1.5\ m,\ T_p = 6\ s,\ \gamma = 2.5$)	400	0.1
W_Pier_1	Pierson-Moskowitz ($H_s = 2.0\ m,\ T_p = 7\ s$)	400	0.1
W_Pier_2	Pierson-Moskowitz ($H_s = 3.0\ m,\ T_p = 6\ s$)	400	0.1
W_Bret_1	Bretschneider ($H_s = 4.0\ m,\ T_p = 8\ s$)	400	0.1
W_Bret_2	Bretschneider ($H_s = 0.5\ m,\ T_p = 4\ s$)	400	0.1

process to find the best model architecture for more accurate forecasting [31,32].

In the GMDH network, the Kolmogorov–Gabor polynomial is used to produce a connection between the input and output variables as follows [33]:

$$\widehat{y} = a_0 + \sum_{i=1}^{m} a_i x_i + \sum_{i=1}^{m}\sum_{j=1}^{m} a_{ij} x_i x_j + \sum_{i=1}^{m}\sum_{j=1}^{m}\sum_{k=1}^{m} a_{ijk} x_i x_j x_k + \ldots \tag{9}$$

where m is the number of input variables, $\{x_n\},\ (n = i,j,k)$ is the input variables, $A = (a_0,\ a_1, a_2, \ldots, a_m)$ is the coefficients. $\widehat{y}$ is the output of the network.

2.3. 3. Long short-term memory network

Ref. [34] proposed the LSTM network, which can model the long-term dependency and specify the optimal time delay for the time series systems [35]. LSTM can be used to forecasts the future of time-series data. The architecture of the LSTM consists of an input layer (input gate), a recurrent hidden layer (as a memory block) and an output layer (output gate). There are memory cells in the hidden layer which has self-connection and retaining the time state. Moreover, there is adaptive multiplications gating unity, which is responsible for controlling data flow through the memory block. The self-connected linear unit-Constant Error Carousel (CEC) is the core of the memory block and the activity of CEC shows the cell statues. In this network, the considered output is computable via Eqs. (5-10) as follows:

$$i_t = \sigma(W_{ix} x_t + W_{im} m_{t-1} + W_{ic} c_{t-1} + b_i) \tag{10}$$

$$f_t = \sigma\left(W_{fx} x_t + W_{fm} m_{t-1} + W_{fc} c_{t-1} + b_f\right) \tag{11}$$

$$c_t = f_t \odot c_{t-1} + i_t \odot g(W_{cx} x_t + W_{cm} m_{t-1} + b_c) \tag{12}$$

$$o_t = \sigma(W_{ox} x_t + W_{om} m_{t-1} + W_{oc} c_{t-1} + b_o) \tag{13}$$

$$m_t = o_t \odot h(c_t) \tag{14}$$

$$y_t = W_{ym} m_t + b_y \tag{15}$$

here, $\odot$ is the scalar product of two vectors, c_t is the activation vector of every cell, m_t represents the activation vector of the memory block and weight matrix W via bias vector b are used for connecting the input layer, memory block and output layer. The output of the input gate, forget gate and output gate are also shown by i_t f_t, and o_t, respectively. Symbols of g and h are hyperbolic tangent functions. Parameter σ is the standard logistics sigmoid function as follows:

$$\sigma(x) = \frac{1}{1 + e^{-x}} \tag{16}$$

2.3. 4. Model performance evaluation

Four criteria, including Mean Absolute Error (*MAE*), Root Mean Square Error (*RMSE*), correlation coefficient (*R*), and Scatter Index (*SI*), are employed to evaluate the performance of the studied forecasting methods. Closer values of *MAE*, *RMSE* and *SI* to 0 and closer value of R^2 to 1 show the higher agreement between the target and the forecasted values. These criteria are calculated as follows [36–38]:

$$MAE = \frac{1}{n}\sum_{i=1}^{n} |T_i - O_i| \tag{17}$$

$$RMSE = \sqrt{\frac{1}{n}\sum_{i=1}^{n} (T_i - O_i)^2} \tag{18}$$

$$R^2 = \left(\frac{\sum_{i=1}^{n}(T_i - \overline{T})(O_i - \overline{O})}{\sqrt{\sum_{i=1}^{n}(T_i - \overline{T})^2 \sum_{i=1}^{n}(O_i - \overline{O})^2}}\right)^2 \tag{19}$$

$$SI = \sqrt{\frac{\sum_{i=1}^{n}((T_i - \overline{T}) - (O_i - \overline{O}))^2}{\sum_{i=1}^{n} T_i^2}} \tag{20}$$

where n is the total number of instances of the studied data set, while T_i and O_i are i^{th} target (obtained from real measurements) and output (obtained from forecasting models) value of the wave excitation force, respectively. $\overline{T}$ and $\overline{O}$ are the mean of the target and the output of the wave excitation force data sets, respectively. The forecasting models having the minimum error and maximum R^2 are chosen as the best model.

2.4. Wave elevation data sets

As aforementioned, the wave excitation force is related to the wave elevation. It can be said that different wave elevation records lead to different wave excitation forces. Therefore, it is needed to create some time-series of wave elevation records to compare the

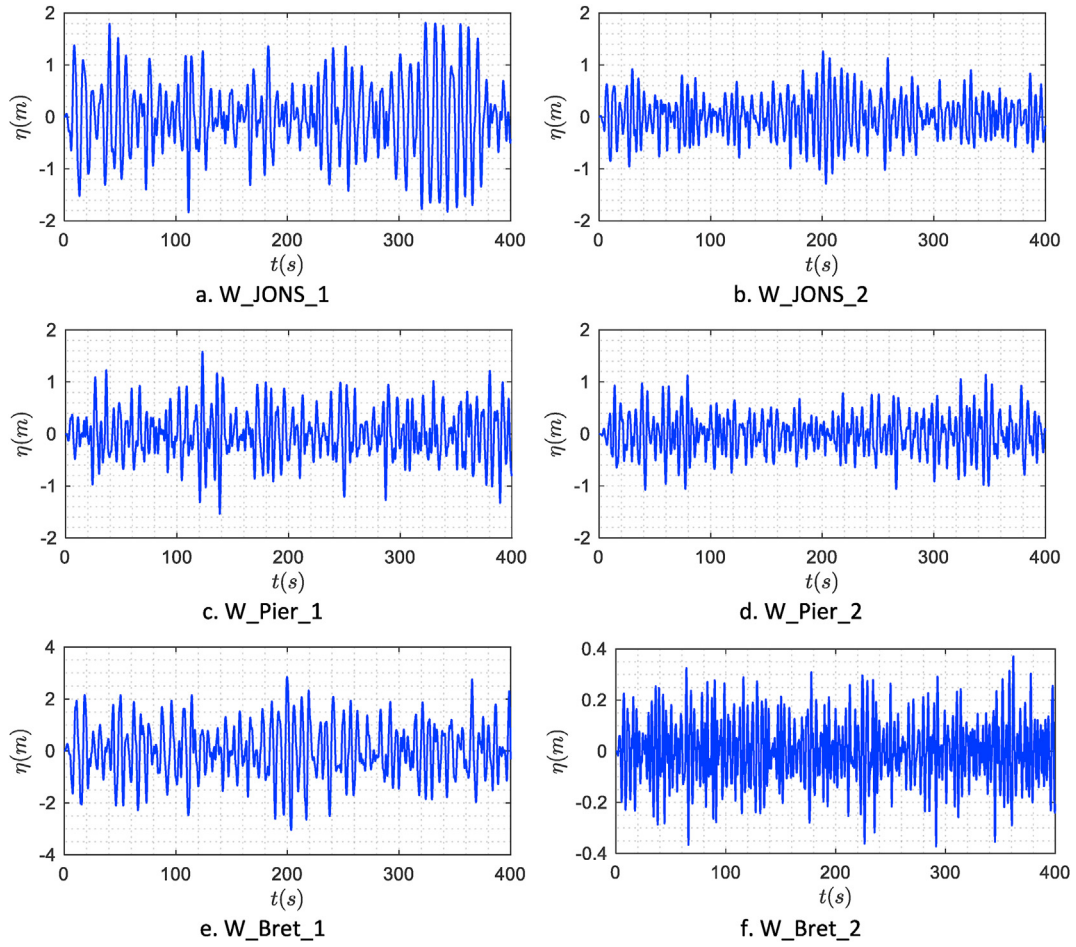

Fig. 3. Time-series of the wave elevation records that act on the bodies of the considered WEC device.

performance of the studied forecasting methods at a variety of wave conditions. Here, the JONSWAP [39], Pierson-Moskowitz [40], and Bretschneider [41] spectrums are used to generate different irregular incident wave conditions which act on the bodies of the WEC device. The target values of the wave excitation force obtained from Eq. (3) are calculated based on the generated wave elevation records. The wave surface elevation is calculated at the origin of the coordinate system that is used for the hydrodynamic analysis of the considered WEC. The origin of the body coordinate system is considered at the center of gravity. In real applications, the wave elevation has to be measured at a certain point. It is more realistic to put the wave gauge at a distance away from the WEC, so that it measures the incoming waves. Moreover, such measurement will only be up to the current time t.

The details of the considered wave elevation records are presented in Table 1. Moreover, the time-series of the wave elevation records and the related spectrums are depicted in Fig. 3 and Fig. 4, respectively. As seen from these figures, it is clear that the considered waves are selected from a wide range of sea wave conditions.

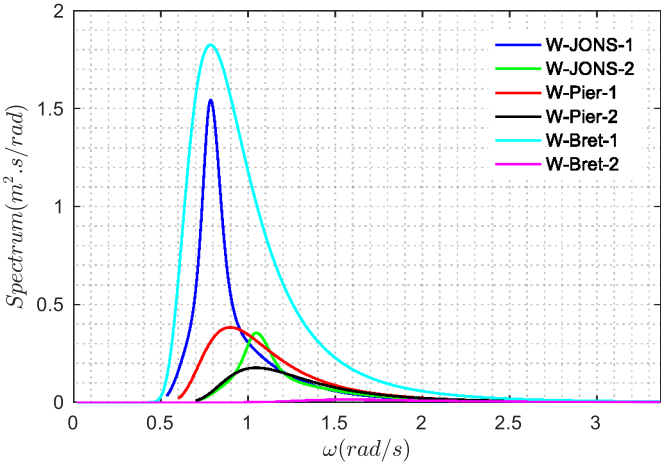

Fig. 4. The spectrum of the wave elevation records that act on the bodies of the considered WEC device.

3. Results and discussions

In this section, the performances of the forecasting models are presented for different wave elevation records described in subsection 2.4. Indeed, the target excitation force values from Eq. (3) are compared to the excitation force values calculated using forecasting models. To this end, the dynamic model of the WEC device must be created first.

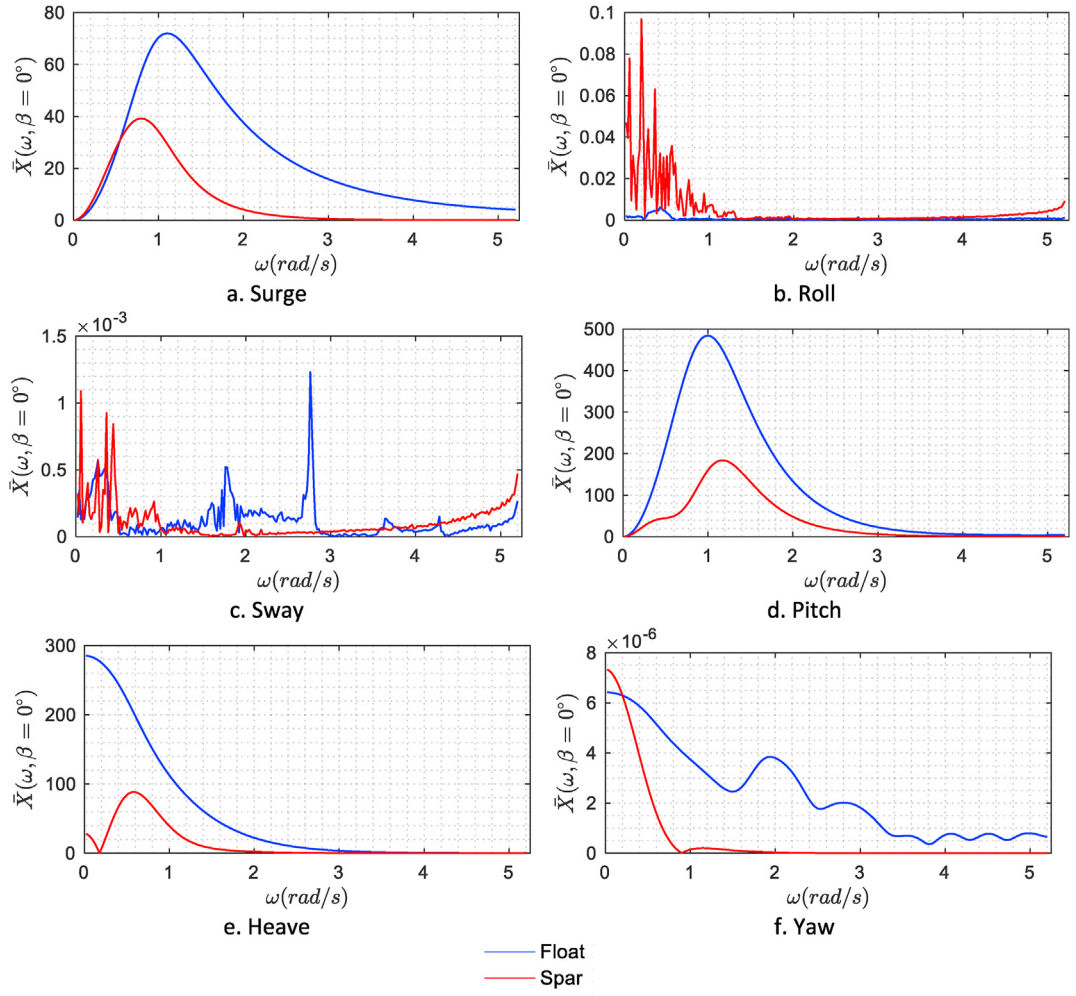

Fig. 5. Normalized excitation force magnitudes $\overline{X}(\omega, \beta) = X(\omega, \beta)/\rho g$ of the considered WEC bodies at all freedom-degrees.

3.1. Hydrodynamic analysis

The hydrodynamic model of the considered WEC is based on the linear potential flow theory, which assumes that the fluid is inviscid, irrotational and incompressible. The frequency-dependent terms, such as added mass, wave excitation and radiation damping are obtained from the boundary element code WAMIT software [42]. The results obtained from the frequency-domain analysis are used in the time-domain analysis. The time-domain simulation of the WEC movements is performed using the WEC-Sim code [43], which is developed by the Sandia National Laboratories and the National Renewable Energy Laboratory.

In the simulations, $\beta = 0^{\circ}$ and $\rho = 1025\ kg/m^3$ are considered. Moreover, the hydrodynamic interaction between the spar and floating body is not considered due to simplification of the WEC hydrodynamic modeling and reduce the code running time and computational cost. The frequency-domain analysis results of the excitation force are presented in Figs. 5–7. The normalized wave excitation magnitudes correspond to the considered WEC bodies at all freedom-degrees is shown in Fig. 5 as a function of angular frequency. Moreover, Figs. 6 and 7 show the excitation force phase and the normalized IRF, respectively. The IRF is calculated from $t = -157\ s$ to $t = 157\ s$ with 1001 number of time steps. Moreover, the frequency range is 0.02 rad/s to 5.2 rad/s. The number of frequency steps used in the IRF calculation is considered as 1001. The interpolation method is adopted for unknown required values. It should be noted that, here, it is assumed that the bodies only move in the heave direction. Figures from the other freedom-degrees are presented for interested readers and providing additional information for other related research.

3.2. Target values of the excitation force

After generation of the wave elevation time-series and frequency and time domain hydrodynamic modeling of the WEC, it is possible to calculate the target values of the wave excitation force using Eq. (3). Wave excitation estimation relies on the knowledge of the wave elevation time history as well as the IRF of the device bodies in the freedom degrees, both of which are known before excitation estimation from previous steps. The time-domain

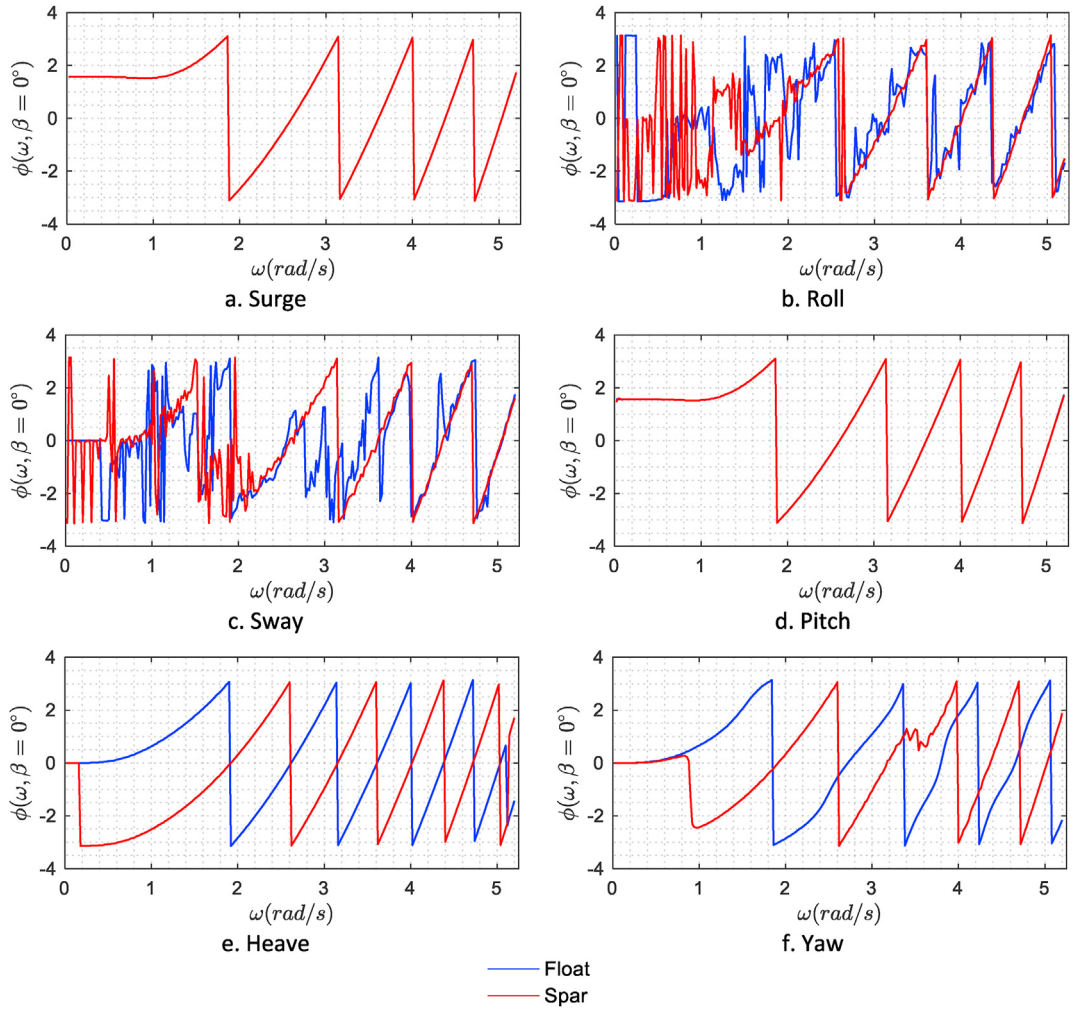

Fig. 6. Excitation force phase $\varnothing(\omega, \beta)$ of the considered WEC bodies at all freedom-degrees.

estimation of the wave excitation force values in the heave direction acted on the considered WEC bodies is shown in Fig. 8. These time-series values are obtained based on the wave elevation records described in subsection 2.4. As seen from Fig. 8, it is clear that the wave excitation force of the floating body is relatively higher than that of the spar body for all studied wave conditions.

3.3. Performance of the forecasting methods

In this section, the three studied forecasting methods presented in this research are evaluated using the different wave climate described in subsection 2.4. The sensitivity of the algorithms to the forecasting horizon and algorithm parameters are studied. First, wave elevation time series are forecasted using studied algorithms. Ten, the excitation force values are calculated from the forecasted values and hydrodynamic coefficients of the WEC based on Eq. (3). To apply forecasting algorithms, each wave elevation data set is divided into two parts, including training (0–390 s) and test (390–400 s) sets. Training data sets are used to create forecasting models to get the best performance with minimum errors.

In contrast, test data sets are used to evaluate the performance of the developed models in future time steps. The statistical details about the wave elevation training and test data sets are presented in Table 2. It should be noted that the performance results of all the studied algorithms presented in the tables are rounded to five digits.

3.3. 1. NAR network

The performance of the NAR network is related to the configuration of the network structure and different algorithm input parameters such as the number of feed-back delays, number of hidden neurons and training method. For the same algorithm input parameters, multiple times training will produce different outputs due to different initial conditions and sampling. Here, a heuristic approach [44,45] is used to achieve the best NAR network structure. In fact, to obtain the best and reliable results, various network

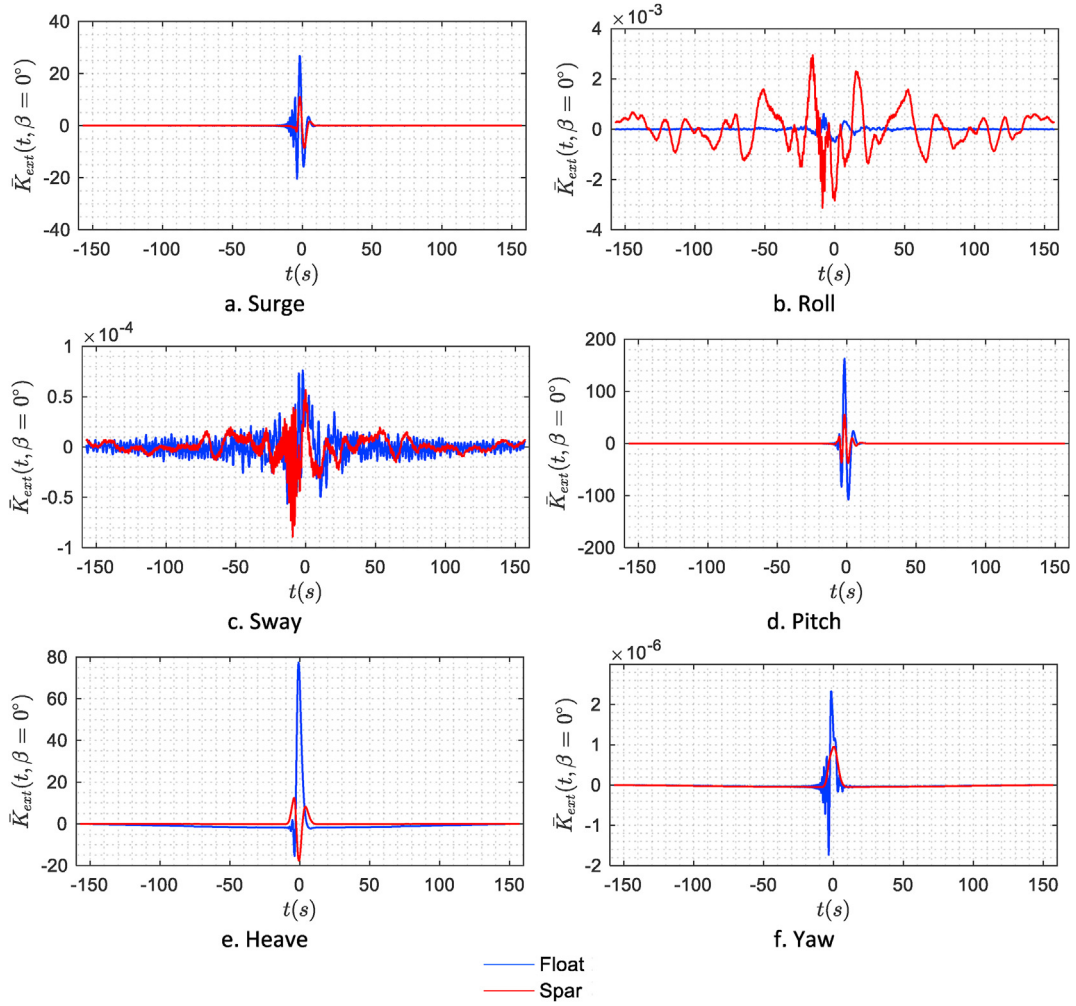

Fig. 7. Normalized excitation impulse response function $\overline{K}_{ext}(t) = K_{ext}(t)/\rho g$ of the considered WEC bodies at all freedom-degrees.

structures are developed based on the input parameters of the algorithm. Then for each wave elevation data set from the developed networks, the best NAR model is selected for forecasting the ahead wave excitation force time series.

To develop the NAR models, LM, BR and SCG are selected as back-propagation training algorithms. According to the MATLAB manual [46], LM algorithm typically requires more memory, but less time is needed for network training. BR method typically requires more training time, but has a good generalization in small or noisy data sets, and SCG requires less memory. Another important NAR structure parameter is the number of hidden neurons. Here, four values, i.e., 5, 7, 10, and 12, are considered for the number of hidden neurons. Moreover, 2 delays are selected in the training phase. For training the networks and avoiding the overfitting, each training wave elevation data set is partitioning randomly into a training set (70% of the data set), a test set (15% of the data set), and a validation set (15% of the data set). Since the modeling is performed using the neural network toolbox of the MATLAB, other algorithms input parameters are considered as default values defined in the software.

Table 3 shows the best NAR network results with different structures for the training wave elevation data sets. The results of the training phase presented in Table 3 show that in all cases, the accuracy of the developed models is high, with a slight difference. In fact, the wave elevation values obtained from the training phase are very close to the real values described in Table 1. Generally, it can be said that in the training data sets, differences in the number of hidden neurons and training algorithms do not lead to the results with noticeable differences. For most cases, the best performance belongs to LM training algorithm with 10 hidden neurons, while the SCG algorithm presents the lowest accuracy.

Now it is possible to calculate the forecasted wave excitation force values for training wave data sets using the best developed NAR network models obtained in Table 3. The performance indicators of the forecasted training wave excitation force data sets for floating and spar bodies based on the best developed NAR network models are presented in Table 4. As visible from this table, the excitation force values of the WEC bodies obtained in the training phase are very close to the real values.

After creating the best NAR models based on the wave elevation

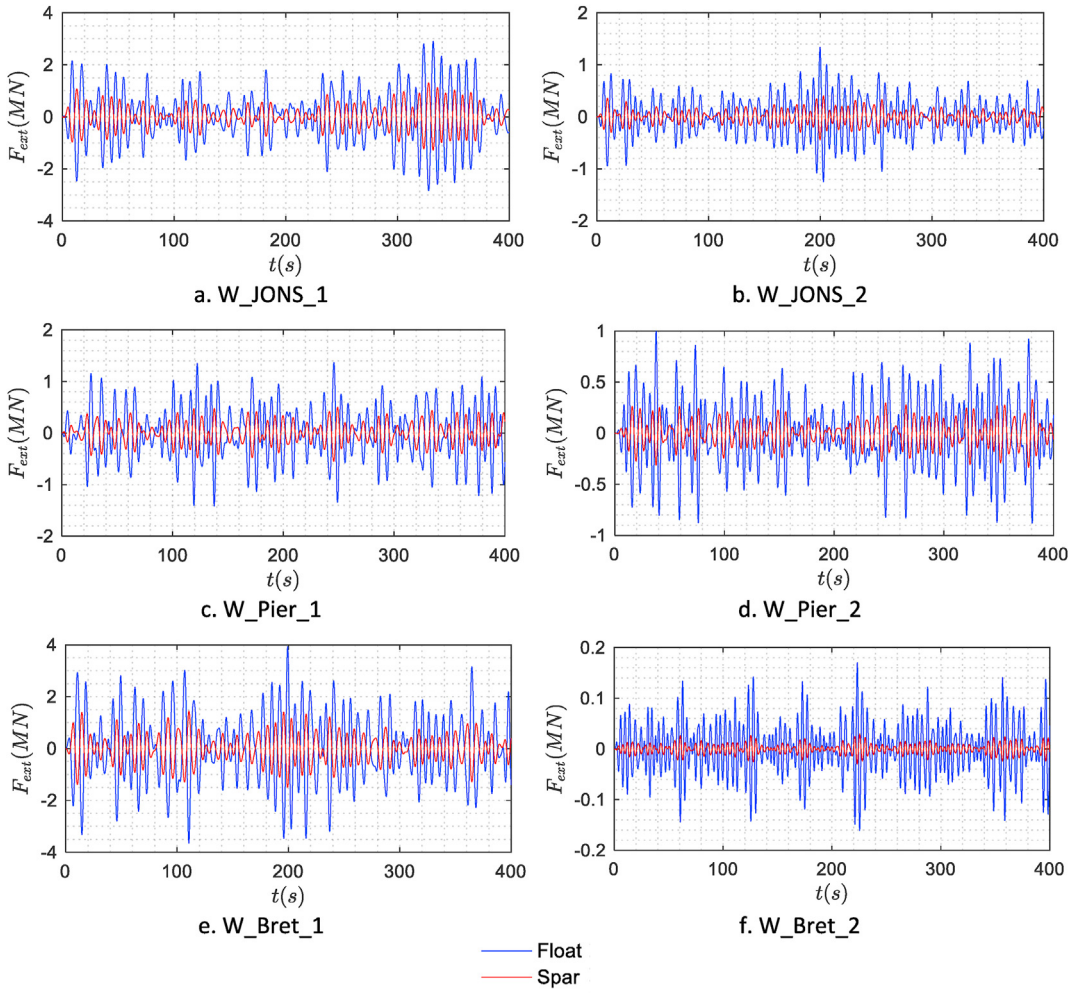

Fig. 8. Time-series of the wave excitation force values in the heave direction act on the bodies of the considered WEC device.

Table 2
The statistical details about the wave elevation training and test data sets used in the forecasting models generation.

Data set	Type	Number of samples	Minimum	Maximum	Mean	Median	Standard deviation
W_JONS_1	Training	3901	−1.83267	1.81201	−0.00097	−0.00886	0.70729
	Test	100	−0.49592	0.69597	0.02216	0.00969	0.33111
W_JONS_2	Training	3901	−1.28701	1.26165	−0.00102	0.00993	0.39252
	Test	100	−0.47947	0.62959	0.00922	−0.01809	0.33335
W_Pier_1	Training	3901	−1.53808	1.58048	−0.00241	−0.02719	0.44976
	Test	100	−0.81085	0.99646	0.05056	0.05428	0.55206
W_Pier_2	Training	3901	−1.07170	1.14008	−0.00063	0.00516	0.37049
	Test	100	−0.55246	0.42979	0.00725	0.06345	0.27674
W_Bret_1	Training	3901	−3.03805	2.84594	−0.00124	−0.01924	1.01356
	Test	100	−1.14948	2.30104	0.22217	0.02518	0.86494
W_Bret_2	Training	3901	−0.37175	0.37124	−0.00013	−0.00092	0.12010
	Test	100	−0.24048	0.25571	−0.00357	−0.00152	0.14148

data training data sets, it is possible to forecast the wave elevation in the future time steps. It can be said that the models are reliable if their accuracy and generalizability on the test data are acceptable. Here, four multi-step ahead forecasting intervals, i.e., 10, 30, 70, and 100 steps, are considered to evaluate the performance and generalizability of the best developed models for future times. The developed NAR models are simulated in the open-loop form, and then the networks and their final delay states are converted to closed-loop form to perform multi-step forecasting. The forecasting wave elevation and related wave excitation force results for test data sets based on the best developed NAR network models are summarized in Table 5 and Table 6, respectively. Moreover, a comparison between the target and the forecasted wave elevation values for 100-step ahead data sets is shown in Fig. 9. As evident

Table 3
The results of the NAR network with different structures for the training wave elevation data sets (*MAE* and *RMSE* units are *m*).

Data set	Training algorithm	$n = 5$				$n = 7$				$n = 10$				$n = 12$			
		MAE	*RMSE*	R^2	*SI*	*MAE*	*RMSE*	R^2	*SI*	*MAE*	*RMSE*	R^2	*SI*	*MAE*	*RMSE*	R^2	*SI*
W_JONS_1	LM	0.00430	0.00545	0.99994	0.00770	0.00426	0.00540	0.99994	0.00764	0.00426	0.00541	0.99994	0.00764	0.00425	0.00540	0.99994	0.00764
	BR	0.00427	0.00542	0.99994	0.00766	0.00432	0.00547	0.99994	0.00773	0.00428	0.00544	0.99994	0.00768	0.00424	0.00540	0.99994	0.00763
	SCG	0.00662	0.00869	0.99985	0.01229	0.00810	0.01116	0.99975	0.01578	0.00815	0.01103	0.99976	0.01559	0.00851	0.01093	0.99976	0.01546
W_JONS_2	LM	0.00462	0.00573	0.99979	0.01459	0.00460	0.00572	0.99979	0.01458	0.00458	0.00571	0.99979	0.01455	0.00459	0.00571	0.99979	0.01454
	BR	0.00460	0.00572	0.99979	0.01457	0.00460	0.00572	0.99979	0.01458	0.00461	0.00572	0.99979	0.01458	0.00458	0.00570	0.99979	0.01453
	SCG	0.01044	0.01571	0.99840	0.04002	0.00596	0.00790	0.99959	0.02014	0.00799	0.01107	0.99920	0.02820	0.00702	0.00952	0.99941	0.02425
W_Pier_1	LM	0.00543	0.00668	0.99978	0.01485	0.00543	0.00667	0.99978	0.01483	0.00540	0.00666	0.99978	0.01479	0.00539	0.00665	0.99978	0.01479
	BR	0.00542	0.00667	0.99978	0.01483	0.00542	0.00667	0.99978	0.01483	0.00542	0.00667	0.99978	0.01483	0.00542	0.00667	0.99978	0.01483
	SCG	0.01338	0.01968	0.99815	0.04375	0.01162	0.01702	0.99860	0.03783	0.01204	0.01691	0.99859	0.03759	0.01024	0.01592	0.99875	0.03538
W_Pier_2	LM	0.00520	0.00654	0.99969	0.01764	0.00519	0.00652	0.99969	0.01760	0.00516	0.00650	0.99969	0.01755	0.00517	0.00650	0.99969	0.01755
	BR	0.00520	0.00653	0.99969	0.01763	0.00520	0.00653	0.99969	0.01763	0.00520	0.00653	0.99969	0.01763	0.00520	0.00653	0.99969	0.01763
	SCG	0.00848	0.01224	0.99891	0.03303	0.00721	0.00967	0.99932	0.02609	0.00773	0.01061	0.99918	0.02863	0.01124	0.01532	0.99829	0.04136
W_Bret_1	LM	0.01054	0.01329	0.99983	0.01311	0.01053	0.01325	0.99983	0.01307	0.01047	0.01319	0.99983	0.01301	0.01045	0.01319	0.99983	0.01301
	BR	0.01052	0.01326	0.99983	0.01308	0.01051	0.01325	0.99983	0.01307	0.01053	0.01328	0.99983	0.01310	0.01054	0.01328	0.99983	0.01310
	SCG	0.01675	0.02232	0.99952	0.02202	0.01817	0.02416	0.99943	0.02383	0.01413	0.01933	0.99964	0.01907	0.02059	0.02658	0.99931	0.02622
W_Bret_2	LM	0.00317	0.00400	0.99889	0.03330	0.00318	0.00400	0.99889	0.03330	0.00317	0.00400	0.99889	0.03326	0.00316	0.00399	0.99889	0.03325
	BR	0.00317	0.00400	0.99889	0.03330	0.00317	0.00400	0.99889	0.03327	0.00316	0.00399	0.99889	0.03325	0.00318	0.00401	0.99889	0.03338
	SCG	0.00341	0.00430	0.99872	0.03575	0.00451	0.00611	0.99741	0.05087	0.00448	0.00594	0.99755	0.04948	0.00576	0.00790	0.99570	0.06578

Table 4
The forecasted wave excitation force results for floating and spar bodies based on the best developed NAR network models for all training wave data sets (*MAE* and *RMSE* units are *MN*).

Data set	Floating				Spar			
	MAE	*RMSE*	R^2	*SI*	*MAE*	*RMSE*	R^2	*SI*
W_JONS_1	0.00287	0.00361	0.99999	0.00356	0.00114	0.00142	0.99999	0.00324
W_JONS_2	0.00221	0.00276	0.99998	0.00733	0.00089	0.00109	0.99999	0.00848
W_Pier_1	0.00358	0.00441	0.99998	0.00868	0.00152	0.00186	0.99999	0.00920
W_Pier_2	0.00292	0.00361	0.99997	0.01056	0.00122	0.00148	0.99999	0.01203
W_Bret_1	0.00586	0.00737	0.99999	0.00558	0.00247	0.00309	0.99999	0.00565
W_Bret_2	0.00095	0.00123	0.99989	0.02479	0.00020	0.00026	0.99985	0.02863

Table 5
The forecasted wave elevation results based on the best developed NAR network models for all test wave data sets (*MAE* and *RMSE* units are *m*).

Data set	10-step ahead				30-step ahead				70-step ahead				100-step ahead			
	MAE	*RMSE*	R^2	*SI*	*MAE*	*RMSE*	R^2	*SI*	*MAE*	*RMSE*	R^2	*SI*	*MAE*	*RMSE*	R^2	*SI*
W_JONS_1	0.11162	0.14911	0.92912	0.94494	0.36484	0.44975	0.05618	1.44718	0.49634	0.58359	0.00140	1.63500	0.52341	0.58900	0.00159	1.75503
W_JONS_2	0.06010	0.07757	0.98881	0.17365	0.15507	0.17470	0.92243	0.25663	0.1554	0.18859	0.73191	0.55730	0.13896	0.17112	0.76701	0.51394
W_Pier_1	0.03904	0.05677	0.99575	0.11780	0.17724	0.22248	0.96605	0.24381	0.40936	0.50035	0.63856	0.91088	0.34183	0.43317	0.71272	0.78396
W_Pier_2	0.01148	0.01314	0.98579	0.01593	0.09109	0.12767	0.95838	0.24566	0.14072	0.17727	0.65648	0.59513	0.16561	0.19879	0.56198	0.71006
W_Bret_1	0.27827	0.32265	0.17713	1.21545	0.42426	0.49778	0.24748	2.27817	0.58131	0.70026	0.02515	1.55580	0.78969	0.99007	0	1.09914
W_Bret_2	0.00553	0.00638	0.99504	0.07721	0.03978	0.05246	0.69323	0.66119	0.06096	0.07319	0.57024	0.65348	0.09638	0.12329	0.24268	0.87183

Table 6
The forecasted wave excitation force results for floating and spar bodies based on the best developed NAR network models for all test wave data sets (*MAE* and *RMSE* units are *MN*).

Data set	Body	10-step ahead				30-step ahead				70-step ahead				100-step ahead			
		MAE	*RMSE*	R^2	*SI*	*MAE*	*RMSE*	R^2	*SI*	*MAE*	*RMSE*	R^2	*SI*	*MAE*	*RMSE*	R^2	*SI*
W_JONS_1	Floating	0.04038	0.04801	0.99879	0.15882	0.08797	0.09567	0.99519	0.08740	0.29827	0.38394	0.80870	0.52184	0.30239	0.37182	0.48456	0.77569
	Spar	0.06019	0.06025	0.99999	0.02499	0.04357	0.04698	0.99718	0.08492	0.09701	0.11870	0.76123	0.54231	0.10388	0.12354	0.57542	0.70164
W_JONS_2	Floating	0.35199	0.35239	0.82681	0.24754	0.26022	0.28655	0.87945	1.46769	0.25962	0.31063	0.40522	1.06174	0.20460	0.26385	0.56311	0.84162
	Spar	0.12545	0.12562	0.99640	0.12663	0.08452	0.09399	0.00977	1.47852	0.08454	0.09612	0.34065	0.89313	0.06725	0.08264	0.50028	0.77254
W_Pier_1	Floating	0.28912	0.29404	0.97036	0.10138	0.49709	0.61337	0.27351	0.81933	0.72328	0.81737	0.75805	1.12799	0.67459	0.75147	0.69089	0.95040
	Spar	0.21817	0.21924	0.98154	0.16362	0.14357	0.16092	0.02426	0.71764	0.13137	0.15570	0.46982	1.04420	0.09931	0.13102	0.49292	0.95734
W_Pier_2	Floating	0.22403	0.22712	0.95494	0.26959	0.22924	0.25734	0.01821	1.67765	0.25304	0.26980	0.23116	1.01374	0.20853	0.23553	0.32028	0.89974
	Spar	0.09356	0.09416	0.90325	0.23158	0.05992	0.0675	0.35345	1.61584	0.05302	0.06042	0.21168	0.84759	0.04263	0.05193	0.40989	0.76807
W_Bret_1	Floating	0.82870	0.82916	0.42212	0.08940	0.61206	0.66899	0.89169	2.97733	0.61224	0.71861	0.11007	1.05429	1.15530	1.46826	0.00509	1.03273
	Spar	0.26893	0.26909	0.84204	0.07893	0.15304	0.18549	0.09008	1.13519	0.17547	0.21247	0.50400	0.48089	0.26125	0.3143	0.27498	0.86551
W_Bret_2	Floating	0.01469	0.01638	0.80777	0.85609	0.04100	0.0491	0.09390	0.73082	0.06186	0.07142	0.09852	0.93920	0.06449	0.07338	0.09981	0.95439
	Spar	0.00691	0.00738	0.28380	0.70536	0.00896	0.00995	0.00364	0.69922	0.01457	0.01689	0.18741	0.87708	0.01505	0.01721	0.26073	0.91101

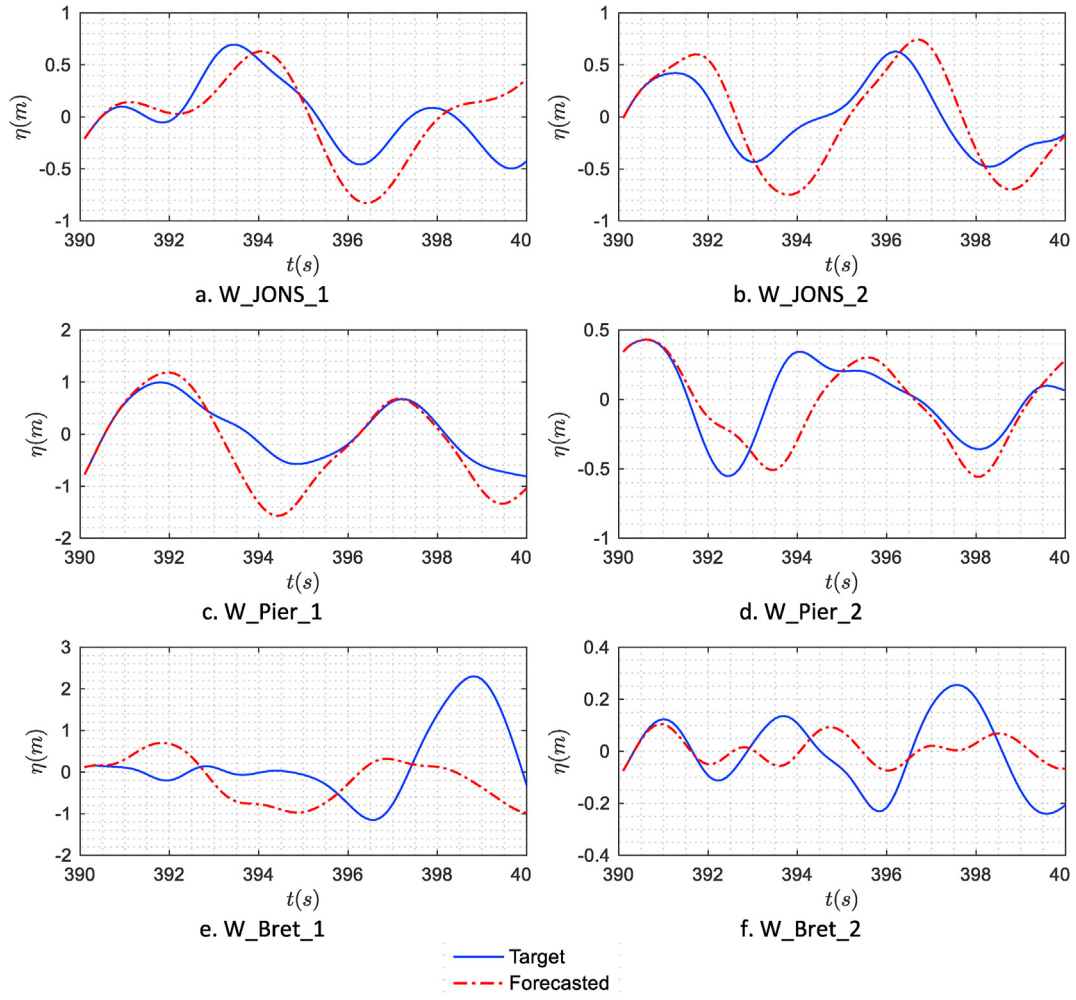

Fig. 9. A comparison between the target and the forecasted wave elevation values based on the best developed NAR network models for 100-step ahead data sets.

from Tables 5 and 6, generally, the developed NAR models can estimate the elevation and wave excitation force in short ahead time steps with high accuracy. It can be said, as the forecasting horizons are increased, the forecasting performance decreases dramatically. In other words, the longer forecasting horizon leads to lower performance.

3.3. 2. *GMDH network*

In this subsection, the performance of the GMDH network is investigated on the forecasting of the wave elevation and wave excitation force data sets. The GMDH MATLAB code is obtained from Ref. [47]. The models input variable is the time series of the wave elevation. Here also, the first 390 s samples of the wave elevation data sets set are used to train the GMDH models and the last 10 s samples are utilized as the test data set to evaluate the generalizability properties of the developed models. Moreover, in the training phase, the training data sets are subdivided into training (70% of the raw data set) and test (30% of the raw data set) sets.

As already mentioned, the GMDH model structure can be configured automatically. The maximum number of neurons in a layer and the maximum number of layers are two main input parameters need to be determined. Here, the network performance is calculated for different network structures, and the most appropriate model input parameters led to the best results are selected as the final structure. Fig. 10 gives the average results of the different developed GMDH network structures for training wave elevation data sets. Due to the random nature of the network and therefore obtaining different results at each algorithm running, the results of Fig. 10 are averaged based on ten times running the GMDH code for each model. The best obtained network structure for each data set is presented in Table 7. Moreover, the performance results of the forecasted training wave excitation force data sets for floating and spar bodies are summarized in Table 8. From these tables, it is evident that there is a significant correlation relationship between the target and forecasted values of all data sets.

To verify the effectiveness and generalizability of the best developed GMDH models, their performance is evaluated on the test wave elevation and excitation force data sets. Table 9 and Table 10 present the forecasting results of the GMDH models for all test wave elevation and wave excitation force data sets in the 10, 30, 70, and 100 ahead time steps, respectively. According to these

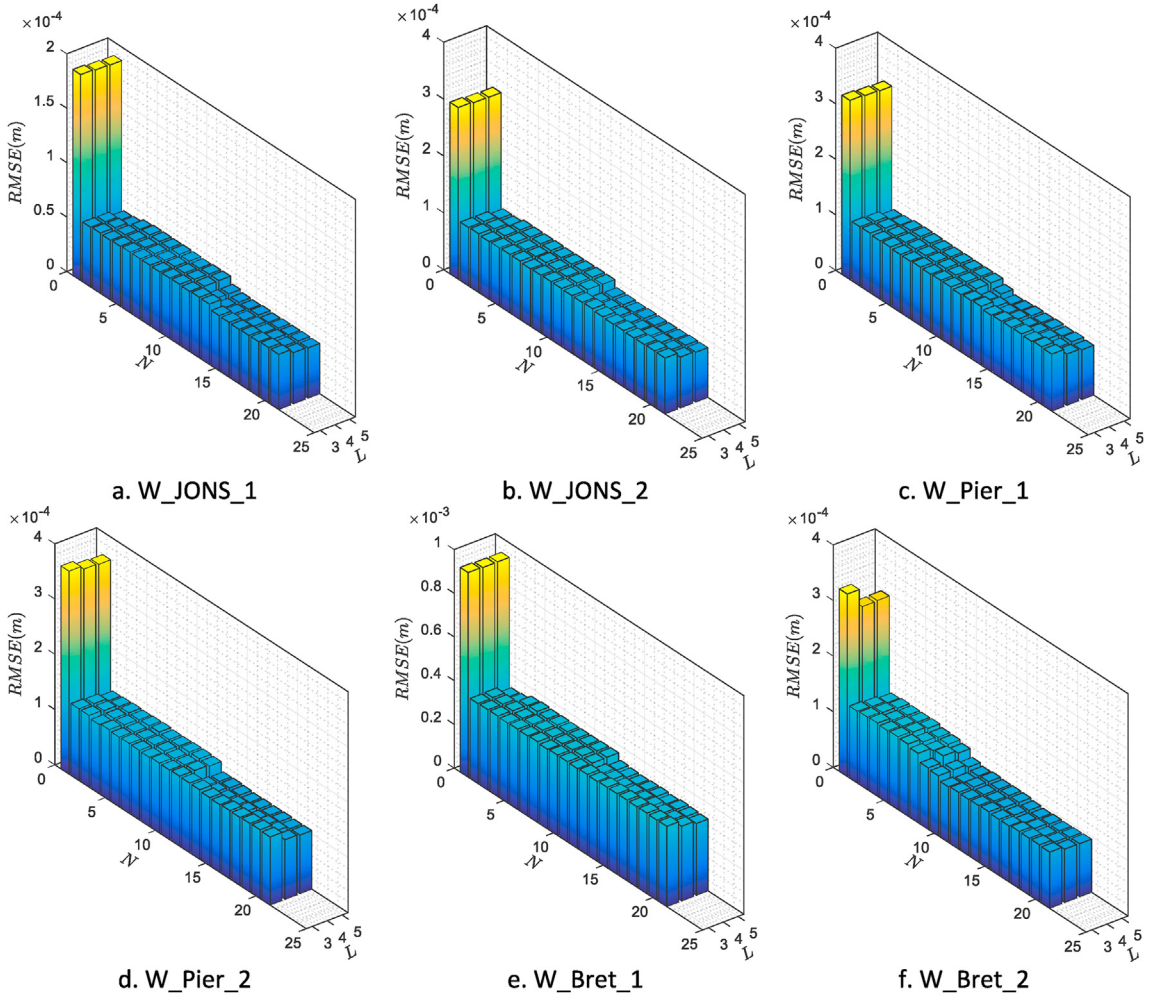

Fig. 10. The average *RMSE* results of the different developed GMDH network structures for training wave elevation data sets based on ten times running the GMDH code (*N*: Maximum Number of Neurons in a Layer, *L*: Maximum Number of Layers).

Table 7
The performance of the best developed GMDH network models for all wave elevation training data sets.

Data set	Maximum number of neurons in a layer	Maximum number of layers	$MAE(m)$	$RMSE(m)$	R^2	*SI*
W_JONS_1	21	5	4.00E-05	4.00E-05	1	6.00E-05
W_JONS_2	22	5	7.00E-05	9.00E-05	1	0.00022
W_Pier_1	18	5	7.00E-05	9.00E-05	1	0.00020
W_Pier_2	20	5	9.00E-05	0.00011	1	0.00029
W_Bret_1	25	5	0.00026	0.00032	1	0.00032
W_Bret_2	21	5	7.00E-05	9.00E-05	1	0.00077

Table 8
The forecasted wave excitation force results for floating and spar bodies based on the best developed GMDH network models for all training wave data sets (*MAE* and *RMSE* units are *MN*).

Data set	Floating				Spar			
	MAE	*RMSE*	R^2	*SI*	*MAE*	*RMSE*	R^2	*SI*
W_JONS_1	0.00541	0.01762	0.99973	0.01657	0.00177	0.01674	0.99855	0.03812
W_JONS_2	0.00028	0.00277	0.99995	0.00737	9.00E-05	0.00114	0.99992	0.00886
W_Pier_1	0.00260	0.00607	0.99988	0.01084	0.00087	0.00643	0.99899	0.03184
W_Pier_2	0.00106	0.01389	0.99835	0.04070	0.00054	0.00500	0.99834	0.04071
W_Bret_1	0.00875	0.02770	0.99960	0.01996	0.00171	0.00919	0.99972	0.01670
W_Bret_2	0.00069	0.00397	0.99363	0.07998	0.00011	0.00057	0.99607	0.06271

Table 9
The forecasted wave elevation results based on the best developed GMDH network models for all test wave data sets (*MAE* and *RMSE* units are *m*).

Data set	10-step ahead				30-step ahead				70-step ahead				100-step ahead			
	MAE	*RMSE*	R^2	*SI*	*MAE*	*RMSE*	R^2	*SI*	*MAE*	*RMSE*	R^2	*SI*	*MAE*	*RMSE*	R^2	*SI*
W_JONS_1	2.61E-02	4.04E-02	0.97445	2.94E-01	0.19958	0.25846	0.20005	0.98931	0.50423	0.61159	0.14339	1.4345	0.52326	0.63555	2.00E-05	1.89626
W_JONS_2	1.35E-02	2.09E-02	0.99362	0.0567	9.61E-02	0.13090	0.94316	0.39584	0.12422	0.14732	0.81267	0.40109	0.12930	0.15161	0.81463	0.45691
W_Pier_1	2.40E-04	2.80E-04	1	0.00057	0.05194	0.11907	0.95276	0.15795	0.19836	0.29586	0.73574	0.53285	0.24721	0.33297	0.65173	0.59510
W_Pier_2	2.69E-02	0.04242	0.33265	0.0818	0.18436	0.24009	0.81423	0.4303	0.23216	0.29459	0.30843	0.99329	0.19599	0.25664	0.44587	0.93160
W_Bret_1	0.05114	0.08417	0.32891	0.49761	0.31903	0.43514	0.57045	2.72382	0.47545	0.61889	0.00378	1.41970	0.69208	0.89759	0.05810	0.98474
W_Bret_2	2.92E-03	3.82E-03	0.99907	0.03148	0.07066	0.09776	0.25457	1.20316	0.12002	0.14447	0.05015	1.32591	0.10766	0.13223	0.30428	0.93593

Table 10
The forecasted wave excitation force results for floating and spar bodies based on the best developed GMDH network models for all test wave data sets (*MAE* and *RMSE* units are *MN*).

Data set	Body	10-step ahead				30-step ahead				70-step ahead				100-step ahead			
		MAE	*RMSE*	R^2	*SI*	*MAE*	*RMSE*	R^2	*SI*	*MAE*	*RMSE*	R^2	*SI*	*MAE*	*RMSE*	R^2	*SI*
W_JONS_1	Floating	4.56E-01	4.57E-01	0.96940	1.21E-01	0.49029	0.5784	0.12365	1.02440	1.04110	1.20658	0.02685	1.76560	0.91502	1.07501	5.35E-02	2.17487
	Spar	3.50E-01	3.50E-01	0.98118	0.10500	2.26E-01	0.25321	0.0367	0.98136	0.32938	0.37121	0.01873	1.75057	0.33018	0.36510	0.02539	2.07637
W_JONS_2	Floating	5.84E-02	6.17E-02	0.77091	0.29252	0.05539	0.06062	0.94001	0.26271	0.13394	0.16905	0.74735	0.50461	0.14359	0.16887	0.77302	0.55878
	Spar	4.54E-02	0.04568	0.02129	0.09372	0.03442	0.03767	0	0.40501	0.05284	0.06141	0.80243	0.52708	0.05574	0.06218	0.84585	0.58118
W_Pier_1	Floating	0.09192	0.11742	0.97916	0.17292	0.38768	0.45217	0.36905	0.36874	0.30515	0.35762	0.7075	0.41862	0.25377	0.30974	0.73922	0.53631
	Spar	2.52E-02	2.96E-02	0.99579	0.19825	0.07388	0.08455	0.52521	0.27592	0.05026	0.06302	0.80822	0.30826	0.05111	0.06225	0.86653	0.44572
W_Pier_2	Floating	0.36999	0.37227	0.94353	0.29774	0.22766	0.25743	0.00444	1.65406	0.13776	0.18303	0.37779	0.93340	0.10970	0.15616	0.51557	0.80539
	Spar	0.09465	0.09523	0.88641	0.23029	0.05793	0.06591	0.27415	1.55008	0.04017	0.05067	0.38637	0.74266	0.02997	0.04256	0.60219	0.63354
W_Bret_1	Floating	0.72372	0.72438	0.81424	0.09984	0.50167	0.55156	0.81968	2.18269	0.49281	0.54518	0.31387	0.78935	0.82697	1.00043	0.34193	0.79026
	Spar	0.17967	0.17981	0.91083	0.06179	0.10317	0.12212	0.13592	0.91731	0.14634	0.18191	0.58775	0.43752	0.20540	0.24776	0.63709	0.68386
W_Bret_2	Floating	0.04167	0.04936	0.84018	1.84402	0.04650	0.05213	0.00035	1.04079	0.05492	0.06552	0.26772	0.84077	0.04577	0.05669	0.49114	0.71393
	Spar	0.00412	0.00479	0.99533	1.28174	0.00766	0.00891	0.56156	0.93472	0.01103	0.01252	0.56412	0.68982	0.00940	0.01108	0.71608	0.58703

Table 11
The performance of the developed LSTM network models for all wave elevation training data sets.

Data set	Number of hidden neurons	*MAE*	*RMSE*	R^2	*SI*
W_JONS_1	250	5.23E-02	6.60E-02	0.99131	9.33E-02
W_JONS_2	250	4.03E-02	5.08E-02	0.98330	0.12950
W_Pier_1	250	4.41E-02	5.61E-02	0.98450	0.12476
W_Pier_2	250	4.10E-02	0.05198	0.98041	0.14033
W_Bret_1	250	0.08628	0.10893	0.98848	0.10748
W_Bret_2	250	1.98E-02	2.51E-02	0.95688	0.20876

Table 12
The forecasted wave excitation force results for floating and spar bodies based on the developed LSTM network models for all training wave data sets (*MAE* and *RMSE* units are *MN*).

Data set	Floating				Spar			
	MAE	*RMSE*	R^2	*SI*	*MAE*	*RMSE*	R^2	*SI*
W_JONS_1	6.33E-02	8.24E-02	0.99341	8.12E-02	0.02707	0.03540	0.99349	0.08067
W_JONS_2	3.53E-02	6.85E-02	0.96736	0.18266	1.22E-02	0.02775	0.95407	0.21615
W_Pier_1	4.22E-02	6.88E-02	0.98226	0.13406	0.01545	0.02842	0.98038	0.14099
W_Pier_2	3.20E-02	0.07074	0.95861	0.20716	0.01088	0.02367	0.96355	0.19250
W_Bret_1	0.09121	0.11308	0.99269	0.08550	0.03649	0.04510	0.99323	0.08229
W_Bret_2	9.03E-03	2.60E-02	0.77799	0.52385	0.00179	0.00689	0.61886	0.75793

tables, the reliable performance is obtained for 10-step ahead forecasting and the performance of other ahead time steps is not acceptable. Here also, the increase in the time steps ahead forecasting leads to a decrease in the accuracy for GMDH models. This problem is due to the very high nonlinear and stochastic properties of the incident wave. Therefore, the ahead time steps must be as low as possible to overcome this problem and increase the accuracy of the forecasting.

3.3. 3. LSTM network

This subsection presents the forecasting results of the wave elevation and excitation force time series data using an LSTM network. The training data sets are normalized for a better fit and to prevent the training from diverging. The number of hidden neurons in the LSTM layer is considered as 250 for all data sets. To train the networks, the Adam optimizer is used as the solver and reduces the learning rate by a factor of 0.2 every 125 epochs with an initial learning rate 0.005. Moreover, the gradient threshold and the maximum number of training epochs are set to 1 and 1500, respectively. Table 11 shows the best obtained network structure for each wave elevation training data set based on ten times running the LSTM code for each model. Moreover, the performance results of the forecasted training wave excitation force data sets for floating and spar bodies are presented in Table 12. Table 13 and Table 14 present the performance of the developed LSTM models to forecast the test wave elevation and wave excitation force data sets. Generally, it can be seen from these tables that the NAR and GMDH models perform better than the LSTM models on the test data sets.

3.4. Methods performance comparison

Table 15 and Table 16 display the overall average performance results of all studied forecasting methods for all training and test wave elevation and wave excitation data sets based on the best developed models, respectively. Based on the comparison results provided in these tables, the GMDH and NAR models provide slightly better results with respect to other compared models in terms of training wave elevation and wave excitation data sets, respectively. In general, the NAR network shows better generalization ability and forecasting accuracy for short-term ahead forecasting of the test data sets. Overall, the performance indicators clearly show the effectiveness of the studied methods to forecast the wave elevation and wave excitation values in the short-term forecasting horizon, here up to 10-step ahead. It is important to note that the performance of the considered methods is not acceptable in some cases, especially for 10-step ahead forecasting. This can be seen especially for wave W_Bret_1. The reason may be the high irregularity degree of this wave because its significant wave height is 4 m, which is higher than the other studied waves. On the other hand, poor results show that considered forecasting methods cannot always achieve the desired results even in short ahead periods of time.

3.5. Sensitivity to the sampling period

The wave elevation sampling period is one of the most important parameters affecting the performance of forecasting methods. Here, W_JONS_1 with a sampling period 0.1–1 s with incremental step 0.1 s is considered to investigate the performance sensitivity of the discussed methods to the wave elevation sampling period. Fig. 11 shows the performance comparison of the three forecasting models for the W_JONS_1 training data set. The configuration of the forecasting models is selected based on the best developed models obtained in subsection 3.3. As seen from Fig. 11, the performance of all developed models is reduced with the sampling period increasing. In other words, the higher sampling period leads to the lower accuracy of the model due to the very high random and nonlinear nature of the incoming waves. Therefore, the sampling period must be performed properly for wave energy applications, especially in the WEC control problems.

Table 13
The forecasted wave elevation results based on the developed LSTM network models for all test wave data sets (*MAE* and *RMSE* units are *m*).

Data set	10-step ahead				30-step ahead				70-step ahead				100-step ahead			
	MAE	*RMSE*	R^2	*SI*	*MAE*	*RMSE*	R^2	*SI*	*MAE*	*RMSE*	R^2	*SI*	*MAE*	*RMSE*	R^2	*SI*
W_JONS_1	1.14E-01	1.46E-01	0.8512	1.31E+00	0.37357	0.46098	0.04786	1.62345	0.45233	0.52561	0.00193	1.48704	0.41842	0.48149	1.48E-03	1.44537
W_JONS_2	4.12E-01	5.18E-01	0.94904	1.18820	8.39E-01	0.92595	0.44237	1.28714	0.87890	0.99222	0.25473	2.94051	0.94061	1.05647	0.16428	3.16734
W_Pier_1	5.19E-01	6.26E-01	0.86293	1.37157	1.07355	1.18937	0.95533	1.16574	0.90883	1.03784	0.93290	1.90364	0.86341	0.99107	0.78046	1.72750
W_Pier_2	6.57E-01	0.69854	0.49939	0.59121	0.61710	0.67893	0.77161	1.29186	0.61544	0.67991	0.21253	2.24893	0.52860	0.60251	0.33101	2.18702
W_Bret_1	0.01836	0.02216	0.07363	0.14206	0.34738	0.46532	0.54120	2.46452	0.36731	0.46593	0.16395	1.01283	0.55293	0.74218	0.29092	0.82048
W_Bret_2	3.77E-01	4.40E-01	0.82574	5.02949	0.34035	0.38503	0.36340	3.74341	0.48239	0.55241	0.25213	4.98873	0.56799	0.64627	0.54734	4.54943

Table 14
The forecasted wave excitation force results for floating and spar bodies based on the developed LSTM network models for all test wave data sets (*MAE* and *RMSE* units are *MN*).

Data set	Body	10-step ahead				30-step ahead				70-step ahead				100-step ahead			
		MAE	*RMSE*	R^2	*SI*	*MAE*	*RMSE*	R^2	*SI*	*MAE*	*RMSE*	R^2	*SI*	*MAE*	*RMSE*	R^2	*SI*
W_JONS_1	Floating	7.60E-01	7.61E-01	0.96043	1.15E-01	0.52961	0.58386	0.07902	0.97881	0.53536	0.60673	0.00013	1.24971	0.55194	0.60345	6.09E-03	1.32635
	Spar	2.75E-01	2.76E-01	0.97644	0.13029	1.85E-01	0.20579	0.01247	0.91269	0.21285	0.24251	0.00104	1.20217	0.20917	0.23157	0.00400	1.31853
W_JONS_2	Floating	1.82E+00	1.83E+00	0.16039	1.52946	1.21646	1.37061	0.71702	4.85346	1.09738	1.21702	0.00013	4.12915	0.87573	1.04647	0.03724	3.36456
	Spar	5.30E-01	0.53055	0.44396	0.30921	0.34765	0.38834	0.07634	5.46180	0.35325	0.39546	0.06379	3.69770	0.29413	0.34667	0.01243	3.23546
W_Pier_1	Floating	1.83121	1.84028	0.99091	0.34508	1.28599	1.45049	0.44741	1.20653	1.04015	1.18252	0.76598	2.42604	1.04854	1.16223	0.37278	2.15815
	Spar	5.19E-01	5.20E-01	0.98303	0.25686	0.35365	0.39389	0.02287	1.35550	0.37320	0.4204	0.45454	2.88365	0.34414	0.38720	0.11240	2.84876
W_Pier_2	Floating	1.09510	1.10751	0.93733	1.19504	0.65449	0.75102	0.09207	4.79111	0.41021	0.53424	0.01091	2.70473	0.40094	0.49410	0.12804	2.53537
	Spar	0.27741	0.28181	0.90500	1.08358	0.17881	0.20195	0.55361	4.96492	0.12037	0.15288	0.02198	2.25330	0.10502	0.13383	0.05190	1.97305
W_Bret_1	Floating	0.77377	0.78070	0.97986	0.33478	0.65101	0.70019	0.14919	1.20993	0.48254	0.58018	0.33178	0.76049	0.78033	0.95086	0.36434	0.78504
	Spar	0.18024	0.18280	0.99421	0.26336	0.19559	0.19782	0.95610	0.30351	0.17640	0.18408	0.67541	0.38777	0.22770	0.24787	0.63909	0.68483
W_Bret_2	Floating	0.48601	0.49704	0.97882	6.01226	0.29444	0.33837	0.92211	6.73278	0.30359	0.34029	0.65821	4.48866	0.31653	0.35332	0.74257	4.47210
	Spar	0.09506	0.09717	0.97919	5.51673	0.05540	0.06437	0.14991	7.85753	0.06774	0.08670	0.26866	4.36664	0.07272	0.08885	0.48003	4.69283

Table 15
The overall average of performance results of all studied forecasting methods for all training and test wave elevation data sets based on the best developed models (*MAE* and *RMSE* units are *m*).

a. Training data sets

Method	*MAE*	*RMSE*	R^2	*SI*
NAR	0.00551	0.00691	0.99965	0.01680
GMDH	0.0001	0.00012	0.99999	0.00031
LSTM	0.0528	0.06676	0.98560	0.11907

b. Test data sets

Method	10-step ahead				30-step ahead				70-step ahead				100-step ahead			
	MAE	*RMSE*	R^2	*SI*	*MAE*	*RMSE*	R^2	*SI*	*MAE*	*RMSE*	R^2	*SI*	*MAE*	*RMSE*	R^2	*SI*
NAR	0.08434	0.10427	0.84527	0.42416	0.20871	0.25414	0.64063	0.85544	0.30735	0.37054	0.43729	0.9846	0.34265	0.41757	0.3810	0.95566
GMDH	0.02013	0.03200	0.77145	0.16036	0.15361	0.21357	0.62254	0.9834	0.27574	0.35212	0.34236	1.01789	0.31592	0.4011	0.37911	0.96676
LSTM	0.34956	0.40845	0.67699	1.60542	0.59849	0.68426	0.5203	1.92935	0.61753	0.70899	0.30303	2.43028	0.64533	0.75333	0.35258	2.31619

Table 16
The overall average of performance results of all studied forecasting methods for all training and test wave excitation data sets based on the best developed models (*MAE* and *RMSE* units are *MN*).

a. Training data sets

Method	Floating body				Spar body			
	MAE	*RMSE*	R^2	*SI*	*MAE*	*RMSE*	R^2	*SI*
NAR	0.00307	0.00383	0.99997	0.01008	0.00124	0.00153	0.99997	0.01121
GMDH	0.00313	0.01200	0.99852	0.02924	0.00085	0.00651	0.99860	0.03316
LSTM	0.04551	0.07159	0.94539	0.20241	0.01731	0.02787	0.91726	0.24509

b. Test data sets

Method	Body	10-step ahead				30-step ahead				70-step ahead				100-step ahead			
		MAE	*RMSE*	R^2	*SI*	*MAE*	*RMSE*	R^2	*SI*	*MAE*	*RMSE*	R^2	*SI*	*MAE*	*RMSE*	R^2	*SI*
NAR	Floating	0.29149	0.29452	0.83013	0.28714	0.28793	0.32850	0.52532	1.29337	0.36805	0.42863	0.40195	0.95313	0.43498	0.52739	0.36062	0.9091
GMDH		0.29028	0.29702	0.88624	0.47134	0.28487	0.32539	0.3762	1.0889	0.36095	0.42116	0.40685	0.87539	0.38247	0.46115	0.48573	0.92992
LSTM		1.12768	1.13609	0.83462	1.5886	0.77200	0.86576	0.40114	3.29544	0.64487	0.74350	0.29452	2.62646	0.66234	0.76841	0.27518	2.44026
NAR	Spar	0.12887	0.12929	0.8345	0.22185	0.08226	0.09414	0.2464	0.95522	0.09266	0.11005	0.41246	0.78087	0.09823	0.12011	0.41904	0.82935
GMDH		0.11651	0.11752	0.79847	0.32847	0.08384	0.09540	0.25559	0.84407	0.10500	0.12346	0.52794	0.74265	0.11363	0.13182	0.61552	0.83462
LSTM		0.31279	0.31472	0.88030	1.2600	0.21935	0.24203	0.29522	3.47599	0.21730	0.24701	0.24757	2.46520	0.20881	0.23933	0.21664	2.45891

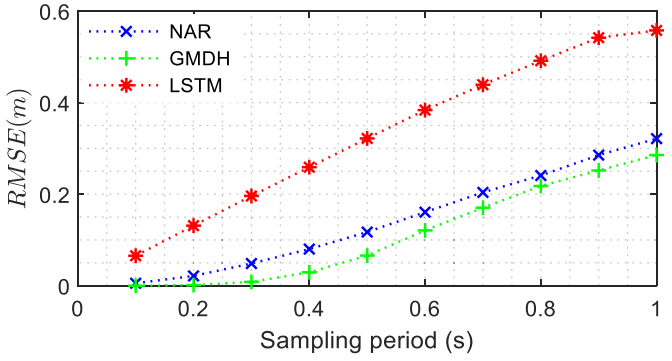

Fig. 11. The sensitivity of the discussed forecasting methods to the wave elevation sampling period, based on the W_Real_1 wave elevation values.

4. Conclusions

In many WEC control strategies, the future values of the wave excitation force are the most important parameter to determine the control input. Many proposed control strategies in the literature simply assume that the excitation force is available, and it can be easily calculated. It is tough to obtain an accurate and reliable wave excitation forecasting model by traditional statistical methods due to the very high non-stationarity and non-linearity nature of the waves. This study is a methodology that uses wave elevation measurements to estimate the excitation forces on the WEC device. Therefore, the main purpose of this paper was to propose a more accurate machine learning-based methodology to forecast the wave excitation force for wave energy conversion applications. To this purpose, three machine learning forecasting methods were tested on the six different irregular wave elevation data sets generated with standard wave spectrums.

The sensitivity of the concerned forecasting methods to the various wave conditions was investigated for a time-domain model of a generic heaving two-body WEC. The obtained results indicated that the performance of all forecasting methods on the training data sets was not much different, and all methods provided acceptable results. But the considered methods gave different results on the different horizon test data sets. In general, the NAR network provided higher accuracy and reliable results than other methods in short-term wave elevation and wave excitation force forecasting. Based on the obtained results, it can be said that the accuracy of the methods decreases significantly if the sampling period increases. Therefore, it should be noted that the acceptable efficiency of the methods is in a short forecasting horizon. Generally, the required forecasting horizon depends on the suboptimal and optimal control displacement and velocity of the device.

The proposed methodology implementation is not challenging and does not require extensive tuning input parameters. The existing methodologies for the wave excitation force forecasting are mainly developed for a typical sea state. This methodology can be applicable to different sea waves of high irregularity in real sea

wave conditions. Moreover, the proposed methodology in the present paper can also be applied to other WEC concepts, an array of the WECs and even other energy maximization control problems. It can be coupled directly to a controller to improve the performance of WEC devices. Although the proposed methodology has some advantages, it is not without limitations. The implementation of these methods requires sufficient historical data sets. Providing such data requires some tools and methods to measure the wave elevation records. As another limitation of this research, the performance of the studied methods on the real wave elevation data and real wave excitation force of a specific WEC has not been investigated. On the other hand, forecasting of excitation force is inherently difficult, since excitation force (a linear concept) is not directly measurable, and it is difficult to get reliable error metrics. Here, a WEC-Sim model with linear hydrodynamics is used. This gives a manageable problem– free surface filtered by a low-pass filter. In fact, even if we used a non-linear model to produce data, there would be some difficulty, since excitation force is not separable from diffraction and buoyancy forces in a non-linear system (for example implemented with CFD).

As future works, it can be examined the proposed forecasting methodology on a real WEC control system and study the different forecasting effects on the output power. Moreover, it is possible to investigate the effects of different real sea conditions, WEC device geometrical parameters, and wave excitation estimation method on the accuracy of the forecasting horizon. As another topic, given that excitation force is synthesized by a low-pass filtered version of the free surface, it's debatable whether the forecasting model for excitation force demands a nonlinear model or not. Another work to improve the forecasting accuracy, it can be trained different networks based on each sea state characteristics, and the algorithm can select the appropriate configuration based on the incident sea state acts on the WEC bodies. On the other hand, to achieve the best ANN structure, some mechanism can be used to replace the heuristic approach by a more structure way such as multi-objective optimization or evolutionary algorithms [48,49]. Moreover, it is possible to use the uncertainty analysis and interval arithmetic [50] to control rounding and truncation errors of the forecasting calculations and thus increasing the accuracy of the created models.

Credit author statement

Kumars Mahmoodi: Writing, Conceptualization; Formal analysis; Investigation; Methodology; Resources; Software; Validation; Visualization; Programming. Erivelton Nepomuceno: Writing – review & editing, Abolhassan Razminia: Writing – review & editing.

Declaration of competing interest

The authors declare that they have no known competing financial interests or personal relationships that could have appeared to influence the work reported in this paper.

Acknowledgments

The authors would like to thank the U.S. Department of Energy's Water Power Technologies Office, National Renewable Energy Laboratory, and Sandia National Laboratories for freely providing WEC-Sim codes. Moreover, the authors also wish to acknowledge Prof. John Ringwood and reviewers for their valuable comments.

References

[1] Wang L, Isberg J, Tedeschi E. Review of control strategies for wave energy conversion systems and their validation: the wave-to-wire approach. Renew Sustain Energy Rev 2018;81:366–79. https://doi.org/10.1016/j.rser.2017.06.074.
[2] Li L, Yuan Z, Gao Y. Maximization of energy absorption for a wave energy converter using the deep machine learning. Energy 2018;165:340–9. https://doi.org/10.1016/j.energy.2018.09.093.
[3] Maria-Arenas A, Garrido AJ, Rusu E, Garrido I. Control strategies applied to wave energy converters: state of the art. Energies 2019;12. https://doi.org/10.3390/en12163115.
[4] Liao Z, Stansby P, Li G. A generic linear non-causal optimal control framework integrated with wave excitation force prediction for multi-mode wave energy converters with application to M4. Appl Ocean Res 2020;97. https://doi.org/10.1016/j.apor.2020.102056.
[5] Shi S, Patton RJ, Liu Y. Short-term wave forecasting using Gaussian process for optimal control of wave energy converters. IFAC-PapersOnLine 2018;51:44–9. https://doi.org/10.1016/j.ifacol.2018.09.467.
[6] Hong Y, Waters R, Boström C, Eriksson M, Engström J, Leijon M. Review on electrical control strategies for wave energy converting systems. Renew Sustain Energy Rev 2014;31:329–42. https://doi.org/10.1016/j.rser.2013.11.053.
[7] Fusco F, Ringwood JV. Short-term wave forecasting for real-time control of wave energy converters. IEEE Trans Sustain Energy 2010;1:99–106. https://doi.org/10.1109/TSTE.2010.2047414.
[8] Fusco F, Ringwood JV. A study of the prediction requirements in real-time control of wave energy converters. IEEE Trans Sustain Energy 2012;3:176–84. https://doi.org/10.1109/TSTE.2011.2170226.
[9] Pena-Sanchez Y, Windt C, Davidson J, Ringwood JV. A critical comparison of excitation force estimators for wave-energy devices. IEEE Trans Control Syst Technol 2019:1–13. https://doi.org/10.1109/tcst.2019.2939092.
[10] Ling BA, Batten BA. Real time estimation and prediction of wave excitation forces on a heaving body. Proc Int Conf Offshore Mech Arct Eng - OMAE 2015;9. https://doi.org/10.1115/OMAE2015-41087.
[11] Garcia-Abril M, Paparella F, Ringwood JV. Excitation force estimation and forecasting for wave energy applications. IFAC-PapersOnLine 2017;50:14692–7. https://doi.org/10.1016/j.ifacol.2017.08.2499.
[12] Pena-Sanchez Y, Garcia-Abril M, Paparella F, Ringwood JV. Estimation and forecasting of excitation force for arrays of wave energy devices. IEEE Trans Sustain Energy 2018;9:1672–80. https://doi.org/10.1109/TSTE.2018.2807880.
[13] Ma Y, Sclavounos PD, Cross-Whiter J, Arora D. Wave forecast and its application to the optimal control of offshore floating wind turbine for load mitigation. Renew Energy 2018;128:163–76. https://doi.org/10.1016/j.renene.2018.05.059.
[14] Hasan Khan MR, Karayaka HB, Yan Y, Tay P, Yu YH. Wave excitation force prediction methodology based on autoregressive filters for real time control. IEEE Green Technol Conf 2019;2019-April. https://doi.org/10.1109/GreenTech.2019.8767127.
[15] Abdelrahman M, Patton R. Observer-based unknown input estimator of wave excitation force for a wave energy converter. IEEE Trans Control Syst Technol 2019;1–8. https://doi.org/10.1109/tcst.2019.2944329.
[16] Shi S, Abdelrahman M, Patton RJ. Wave excitation force estimation and forecasting for WEC power conversion maximisation. IEEE/ASME Int Conf Adv Intell Mechatronics, AIM 2019. https://doi.org/10.1109/AIM.2019.8868870. 2019-July:526–31.
[17] Neary VS, Previsic M, Jepsen RA, Lawson MJ, Yu Y-H, Copping AE, et al. Methodology for design and economic analysis of marine energy conversion (MEC) Technologies. Sandia Natl Lab 2014:261.
[18] Yu Y, Lawson M, Li Y, Previsic M, Epler J, Lou J. Experimental wave tank test for reference model 3 floating- point Absorber wave energy converter project. NREL Rep 2015.
[19] Mahmoodi K, Ghassemi H, Razminia A. Performance assessment of a two-body wave energy converter based on the Persian Gulf wave climate. Renew Energy 2020;12:134–45. https://doi.org/10.1016/J.RENENE.2020.06.071.
[20] Cummins WE. The impulse response function and ship motions. Schiffstechnik 1962;57:101–9. https://doi.org/10.1179/2056711115Y.00000000001.
[21] Liu H, Chen C, Lv X, Wu X, Liu M. Deterministic wind energy forecasting: a review of intelligent predictors and auxiliary methods. Energy Convers Manag 2019;195:328–45. https://doi.org/10.1016/j.enconman.2019.05.020.
[22] Wang H, Liu Y, Zhou B, Li C, Cao G, Voropai N, et al. Taxonomy research of artificial intelligence for deterministic solar power forecasting. Energy Convers Manag 2020;214. https://doi.org/10.1016/j.enconman.2020.112909.
[23] Mahmoodi K, Ghassemi H, Nowruzi H. Data mining models to predict ocean wave energy flux in the absence of wave records. Sci J Marit Univ Szczecin-Zeszyty Nauk Akad Morskiej W Szczecinie 2017;49:119–29. https://doi.org/10.17402/209.
[24] Vaghefi M, Mahmoodi K, Akbari M. Detection of outlier in 3D flow velocity

collection in an open-channel bend using various data mining techniques. Iran J Sci Technol Trans Civ Eng 2019;43:197–214. https://doi.org/10.1007/s40996-018-0131-2.
[25] Vaghefi M, Mahmoodi K, Akbari M. Detection of outlier in 3D flow velocity collection in an open-channel bend using various data mining techniques. Iran J Sci Technol Trans Civ Eng 2019;43. https://doi.org/10.1007/s40996-018-0131-2.
[26] Mahmoodi K, Ketabdari MJ, Vaghefi M. Proposing a new local density estimation outlier detection algorithm: an empirical case study on flow pattern experiments. Pattern Anal Appl 2021. https://doi.org/10.1007/s10044-021-01019-2.
[27] Vaghefi M, Mahmoodi K, Akbari M. A comparison among data mining algorithms for outlier detection using flow pattern experiments. Sci Iran 2018. https://doi.org/10.24200/sci.2017.4182. 0:0–0.
[28] Mahmoodi K, Ghassemi H, Razminia A. Wind energy potential assessment in the Persian Gulf: a spatial and temporal analysis. Ocean Eng 2020;216:107674. https://doi.org/10.1016/j.oceaneng.2020.107674.
[29] Benmouiza K, Cheknane A. Forecasting hourly global solar radiation using hybrid k-means and nonlinear autoregressive neural network models. Energy Convers Manag 2013;75:561–9. https://doi.org/10.1016/j.enconman.2013.07.003.
[30] Ivakhnenko aG. The group method of data handling-a rival of the method of stochastic approximation. Sov Autom Control 1968;13:43–71.
[31] De Giorgi MG, Malvoni M, Congedo PM. Comparison of strategies for multi-step ahead photovoltaic power forecasting models based on hybrid group method of data handling networks and least square support vector machine. Energy 2016;107:360–73. https://doi.org/10.1016/j.energy.2016.04.020.
[32] Jiang Y, Liu S, Peng L, Zhao N. A novel wind speed prediction method based on robust local mean decomposition, group method of data handling and conditional kernel density estimation. Energy Convers Manag 2019;200. https://doi.org/10.1016/j.enconman.2019.112099.
[33] Liu H, Duan Z, Wu H, Li Y, Dong S. Wind speed forecasting models based on data decomposition, feature selection and group method of data handling network. Meas J Int Meas Confed 2019;148. https://doi.org/10.1016/j.measurement.2019.106971.
[34] Hochreiter S, Urgen Schmidhuber J. Long shortterm memory. Neural Comput 1997;9:17351780.
[35] Shahid F, Zameer A, Mehmood A, Raja MAZ. A novel wavenets long short term memory paradigm for wind power prediction. Appl Energy 2020;269. https://doi.org/10.1016/j.apenergy.2020.115098.
[36] Zheng CW, Li CY. Variation of the wave energy and significant wave height in the China Sea and adjacent waters. Renew Sustain Energy Rev 2015;43:381–7. https://doi.org/10.1016/j.rser.2014.11.001.
[37] Mahmoodi K, Ghassemi H, Nowruzi H, Shora MM. Prediction of the hydrodynamic performance and cavitation volume of the marine propeller using gene expression programming. Ships Offshore Struct 2018. https://doi.org/10.1080/17445302.2018.1557589.
[38] Mahmoodi K, Ghassemi H, Razminia A. Temporal and spatial characteristics of wave energy in the Persian Gulf based on the ERA5 reanalysis dataset. Energy 2019;187:115991. https://doi.org/10.1016/j.energy.2019.115991.
[39] Hasselmann K, Barnett TP, Bouws E, Carlson H, Cartwright DE, Eake K, et al. Measurements of wind-wave growth and swell decay during the joint North Sea wave project. JONSWAP); 1973.
[40] Pierson WJ, Moskowitz L. A proposed spectral form for fully developed wind seas based on the similarity theory of S. A. Kitaigorodskii. J Geophys Res 1964;69:5181–90. https://doi.org/10.1029/jz069i024p05181.
[41] Prendergast J, Li M, Sheng W. A study on the effects of wave spectra on wave energy conversions. IEEE J Ocean Eng 2020;45:271–83. https://doi.org/10.1109/JOE.2018.2869636.
[42] WAMIT. User Manual: version 7.0 2013.
[43] Lawson M, Yu Y-H, Ruehl K, Michelen C. Improving and validating the WEC-Sim wave energy converter code. Proc. 3rd Mar. Energy Technol. Symp. 2015 Washington, D.C.
[44] Nepomuceno EG, Neto OM, Takahashi RHC, Tavares CE. A heuristic approach to robust control design for power systems with several FACTS devices. Int J Electr Power Energy Syst 2003;25:13–20. https://doi.org/10.1016/S0142-0615(02)00035-2.
[45] Amaral GFV, Nepomuceno EG. A smooth-piecewise model to the Cord Attractor. Chaos, Solit Fractals 2018;109:31–5. https://doi.org/10.1016/j.chaos.2018.02.001.
[46] Matlab help document n.d. http://www.mathworks.com.
[47] Kalami Heris M. Group method of data handling (GMDH) in MATLAB. 2015.
[48] Nepomuceno EG. A novel method for structure selection of the Recurrent Random Neural Network using multiobjective optimisation. Appl Soft Comput J 2019;76:607–14. https://doi.org/10.1016/j.asoc.2018.10.055.
[49] Ottoni ALC, Nepomuceno EG, de Oliveira MS, de Oliveira DCR. Tuning of reinforcement learning parameters applied to SOP using the Scott–Knott method. Soft Comput 2020;24:4441–53. https://doi.org/10.1007/s00500-019-04206-w.
[50] Priscila Fernanda da Silva Guedes, Márcia Luciana da Costa Peixoto, Otávio Augusto Rodrigues de Oliveira Freitas, Alípio Monteiro Barbosa, Samir Angelo Milani Martins, Erivelton Geraldo Nepomuceno. Interval simulation of narmax models based on computer arithmetic. 2018. https://doi.org/10.20906/CPS/CBA2018-0739.